Field-Orientation Coupling Effects in Nematic Liquid Crystal Cells

by

Jake Ferguson

A thesis
presented to the University of Waterloo
in fulfillment of the
thesis requirement for the degree of
Master of Science
in
Physics

Waterloo, Ontario, Canada, 2019

Author's Declaration

This thesis consists of material all of which I authored or co-authored: see Statement of Contributions included in the thesis. This is a true copy of the thesis, including any required final revisions, as accepted by my examiners.

I understand that my thesis may be made electronically available to the public.

Statement of Contributions

This thesis contains work done using a numerical model codebase, to which I have made major contributions, originated by Fred Fu. Chapter 3 of this thesis contains model equations whose derivations are attributable to Mr. Fu.

All other work in this thesis was performed by myself under the supervision of Professor Nasser Mohiedden Abukhdeir.

Abstract

Using the continuum Landau-de Gennes model for the nematic liquid crystal (NLC) phase, we study the equilibrium behaviour of nematic cells, accounting for the coupling between external fields and nematic order. This is motivated by the substantial past theoretical and computational studies either neglecting or simplifying this coupling. Two different types of NLC cells are studied, those used to measure nematic elasticity through observation of a macroscopic optical response (Fréedericksz transition) and a typical NLC light shutter used in liquid crystal display (LCD) technology.

The Fréedericksz cell and its associated transition are studied, comparing simulation prediction, given phenomenological parameters describing nematic elasticity, to experimental observations. This NLC cell configuration involves a relatively simple imposed electric (or magnetic) field, which is usually approximated instead of numerically determined. Particular emphasis is placed on investigating the impact of typical model approximations and parameter variance on the predicted transition point. We demonstrate that the relative values of the thermodynamic bulk constants has a pronounced effect on the transition voltage. It is shown that the coupling effect becomes significant above the Fréedericksz transition point.

The in-plane switching (IPS) nematic cell is studied, which involves a relatively complex electric field compared to the previous case. Approximation of the electric field is not feasible in this case, highlighting the use of a fully-coupled simulation approach. The effects of electrode placement and use of a fully coupled model versus a decoupled isotropic approximation are studied. A significant discrepancy between the predicted ON-state textures near the lower substrate of the IPS cells between the coupled and uncoupled models is observed. Finally, the utility of the model for the design and optimization of LCD cell systems is demonstrated and discussed.

Acknowledgements

With great appreciation I would like to thank Professor Nasser Mohiedden Abukhdeir whose professional mentorship has been invaluable, and whose interest in the well-being of his students is ever present.

I would also like to thank Fred Fu, whose excellent previous work served as a foundation. Thank you as well to Tanyakarn Treeratanaphitak, James Lowman, Alex Vasile, Victor Guiguer, and Kimia Entezari for your comradery and expertise.

Table of Contents

List of Tables

List of Figures

Chapter 1

Introduction

The desire for simultaneously precise, intricate and yet arbitrary manipulation of light has driven a persistent line of scientific and technical interest. This field has grown from the nascent use of focusing lenses in antiquity to the vast and complex optical manipulation found in modern display and imaging technology. Though the significant breadth of desired control over light creates a highly eclectic ensemble of methods and technologies, the shared core of this pursuit is the exploitation of the physical properties of phases of matter which exhibit anisotropy.

The search for suitable candidate materials in the construction of optical devices is often difficult, with prospective compounds needing to manifest (or absolutely not manifest) multiple properties simultaneously with multiple degrees *and* mechanisms of tunability. Current display technologies require materials which can rotate the polarization of light with tunability faster than the human eye can perceive. Adaptive lenses require materials whose refractive indices can be adjusted continuously without change in transmittance. Adaptive glass technologies require materials which scatter light in one state and transmit it faithfully in another.

Liquid crystalline phases of matter have unique properties that satisfy the above criteria, with their physical and dielectric anisotropies being exploitable for a broad array of purposes. The many different species of liquid crystal molecules, and the degrees of freedom associated with constructing liquid crystal systems, create a broad range of properties which has resulted in their widespread adoption. Liquid crystal displays (LCDs) alone constitute a multi-billion dollar global industry, with many people living the majority of their days within arms reach of at least one liquid crystalline thin film.

Given their ubiquity and utility, it is unsurprising that an immense amount of work has

been done in understanding liquid crystals (LCs) within a rigorous physical framework. Several different models exist to describe the dynamics of these systems, varying in the approximations they make or the phases they describe. As LCs become still further prevalent with emerging technologies in medical imaging and adaptive optics, and with simulation increasingly eclipsing more costly experimentation, understanding explicitly the accuracy and scope of these models becomes a task that transitions from useful to unignorable.

1.1 Objectives

Contemporary models of LC phases vary in the approximations they make and the range of systems they are able to accurately describe. Early models, or models designed for homogeneous LC domains, construct a theory using either scalar or vector order parameters. More general models use a tensor order parameter capable of describing the multiple degrees and directions of ordering present in the phase, and have experienced increased interest as new liquid crystal phases are discovered. In simulations of the LC phase interaction with applied electric or magnetic fields, it is common practice to solve the field portion heuristically. That is, to ignore the coupling between the ordering of the material and the electric field mediated by dielectric anisotropy.

The purpose of this work is to study the effect of coupling between the multiple degrees and directions of ordering in liquid crystals and external electric fields. To this end, a dynamic continuum model is formulated using the Landau-de Gennes free energy of the nematic LC phase and solved using the standard numerical methods for partial differential equations. Simulations are performed for a number of both analytically and industrially relevant systems. The primary objectives of this work are:

1. Construct a numerical solution of the continuum model, building upon an existing uncoupled implementation by Abukhdeir and Fu [15].

2. Validate the model against experimental data and quantify its precision relative to the precision of model parameters and assumptions.

3. Investigate the validity of approximations used in uncoupled models, and identify unique dynamics associated with the interchange between bulk and electric free energies.

4. Demonstrate the utility of the developed model by conducting a study of the design optimization of In-Plane Switching (IPS) LCD cells.

1.2 Thesis Structure

This thesis outlines the derivation of the Landau-de Gennes model, its numerical implementation within a finite element scheme, and the validation of the model against contemporary models and experimental data.

Thermotropic liquid crystals and their properties are outlined in Chapter 2. The physical theory of thermotropic liquid crystals and a description of the numerical methods used by this work is contained in Chapter 3.

With the implemented model and theory described, we study the splay-mode Freedericksz transition in Chapter 4. The model is validated against experimental data and the impact of director-field coupling on transition dynamics is examined.

Having an understanding of model validity and precision, and the impact of coupling on a simple texture, we consider in-plane switching liquid crystal display cells in Chapter 5. The effect of coupling on the pertinent attributes of their design is studied, and the potential of the model for design optimization is established.

Concluding in Chapter 6, we then summarize our findings and comment on the potential for future work.

Chapter 2

Background

2.1 Liquid Crystal Classifications

Liquid crystals (LCs) are a phase of matter intermediate to conventional crystalline solids and isotropic liquids, and exhibit characteristics of both phases. Where crystals are characterized by strong long-range ordering in both molecular position and alignment (*translational* and *orientational* ordering), isotropic liquids exhibit only short-range ordering, and are rotationally and translationally invariant on macroscopic scales. LC molecules, or *mesogens*, exhibit a number of modes of long range order with semi-continuous degree across mechanisms in temperature, concentration, and molecular composition [2, 3].

There exists an immense number of liquid crystal species, with additional members commonly being constructed from well-understood chemical building blocks or being discovered. In this work we focus on rod-like *thermotropic* mesogens, which exhibit a strong physical anisotropy and whose phase transitions are governed by temperature. At low temperatures, these LCs form conventional crystalline solids, melting into multiple intermediary phases or *mesophases* and ultimately an isotropic liquid with increasing temperature [1].

At low temperatures, the *smectic* phases are characterized by the presence of orientational order and translational order of lower dimensionality relative to the crystal phase; LC molecules align in regular planes which are positionally isotropic within themselves. As temperature is varied in the smectic range, preferred molecular orientation (commonly referred to as the *director*) transitions from tilted (Smectic C) to perpendicular (Smectic A) with respect to the molecular planes. With the addition of further thermal energy,

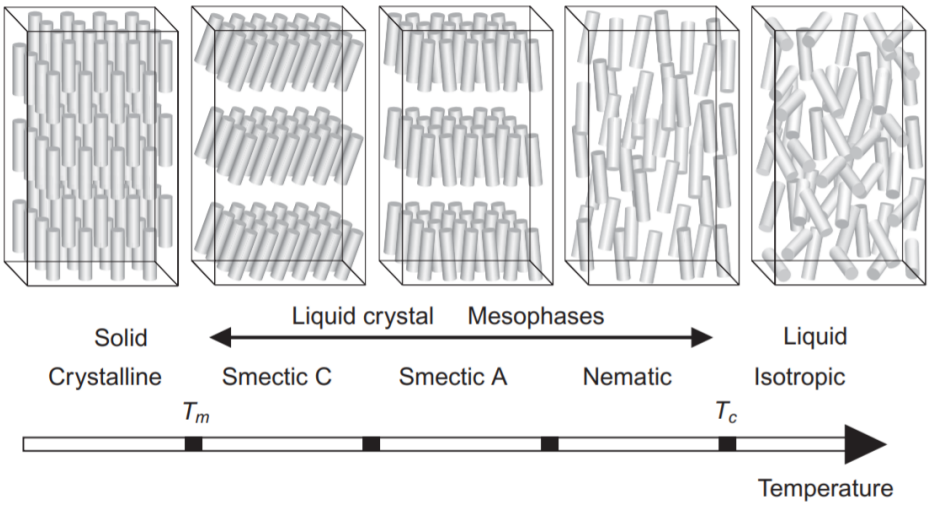

Figure 2.1: Orientational and positional ordering in thermotropic mesophases. From ref [1].

translational ordering is lost and the resulting *nematic* phase exhibits only orientational ordering. Hydrodynamic properties vary significantly between the mesophases, with the positional isotropy granting the nematic lower viscosity. As temperature is still further increased, all long-range ordering is lost and the mesogen becomes disordered, entering a conventional isotropic liquid phase[3, 1]. Figure 2.1 depicts the temperature dependence of thermotropic mesophases.

This work focuses on the nematic phase of thermotropic liquid crystals, which exists at room temperature for many mesogens and is of primary relevance to most LC technology including LCD displays [16].

2.1.1 Molecular Structure

The unique properties of liquid crystals are rooted in their anisotropy at the molecular scale, the structure of which determines the phases they form. Liquid crystal molecules may be conic, discotic, or rod-like in geometry; conic and discotic mesogens are capable of two dimensional columnar ordering whereas rod-like mesogens are capable of orientational and one-dimensional translational ordering as discussed above.

Liquid crystals must exhibit and maintain significant geometric anisotropy, requiring

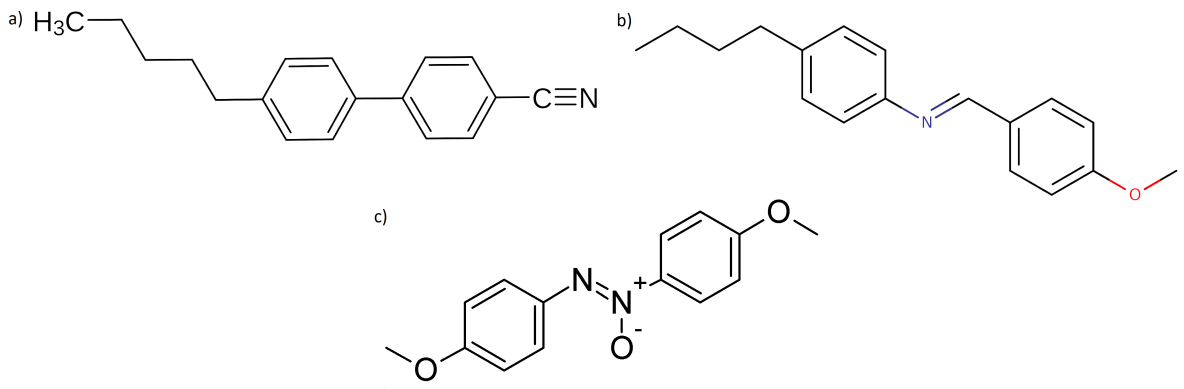

Figure 2.2: Rod-like nematic mesogens. a) 4-Cyano-4'-pentylbiphenyl (5CB) b) N-4-Methoxybenzylidene-4-butylaniline (MBBA) c) para-Azoxyanisole (PAA). From references [60, 61, 62], respectively.

molecules which are both anisometric and highly rigid. Room temperature liquid crystals commonly consist of long alkyl groups (which provide an extended shape) and benzene rings (which provide rigidity) [17, 18].

2.2 Physical Properties

The molecular ordering and physical anisotropy of nematic mesophases imparts them with unique macroscale properties. These properties are the source of practical interest in liquid crystals, with their continuous and tunable nature being highly useful in the engineering of optical devices. While of course intimately related, these properties manifest in a broad array of physical interactions.

2.2.1 Electromagnetic

As in any sufficiently weakly-bonded dielectric material, liquid crystals exhibit a tendency to align (or anti-align, in the case of negative dielectric anisotropy) with an applied external field. Assuming a sufficiently strong field and/or dielectric anisotropy, a torque will be exerted by the dipoles of molecules oblique to the field (Figure 2.4).

The presence of inherent dipoles in the mesogen structure is the key factor in determining the sign of anisotropy and thus the nature of the interaction with applied fields. While

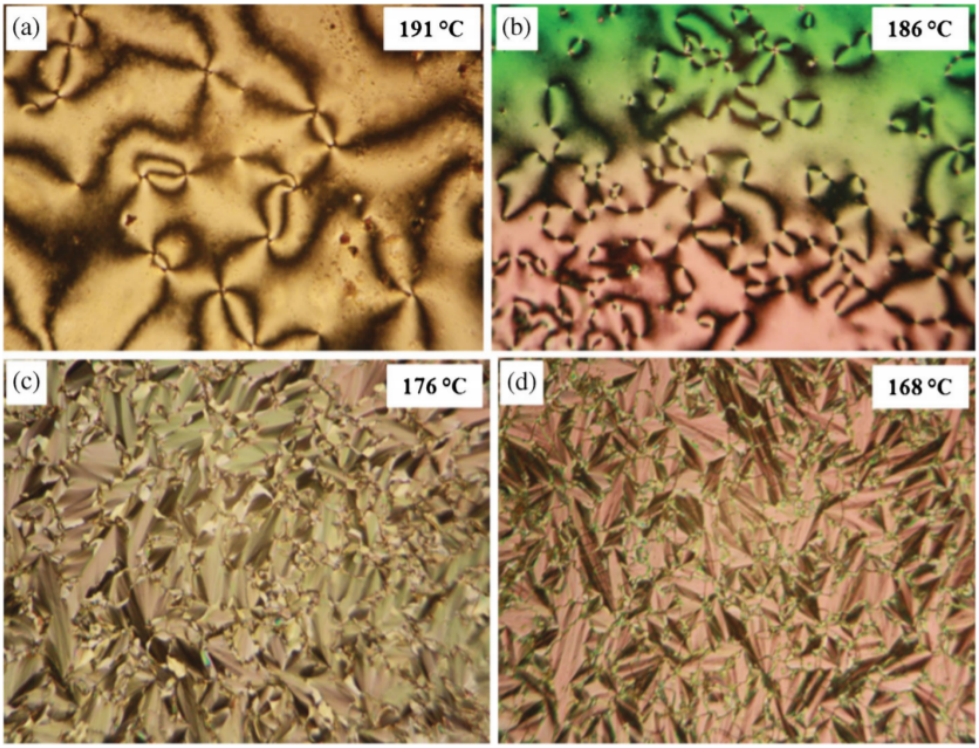

Figure 2.3: Liquid Crystal textures for four different LC compounds viewed under a polarizing optical microscope: a) Nematic phase; b) Nematic phase; c) Smectic A phase; d) Smectic C phase. From ref [8].

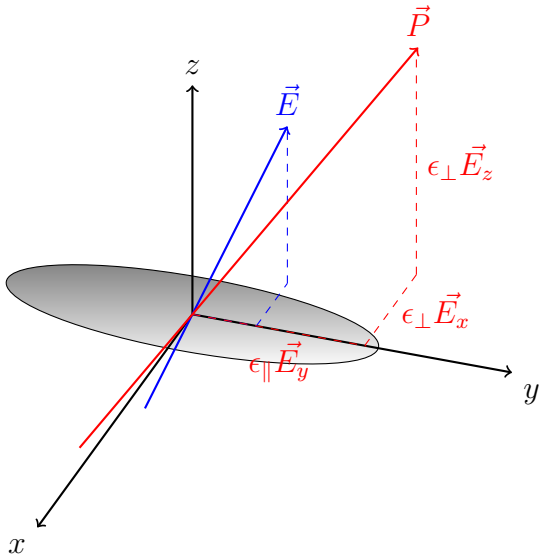

Figure 2.4: Diagram of polarization for LC molecule with positive dielectric anisotropy ($\epsilon_\parallel - \epsilon_\perp > 0$).

the geometric anisotropy of the molecules creates a tendency to create stronger induced dipoles along the molecular axis, sufficiently strong inherent dipoles across the molecular axis may predestine the mesogen for negative anisotropy [19]. The geometric bias towards positive induced dipoles leads to most species exhibiting positive anisotropy. The electric field strength necessary to induce a distortion in the director of a liquid crystalline system is often non-zero due to competition with other alignment interactions including surface effects and elasticity; this is the essence of the *Fréedericksz Transition*, to be discussed in depth in the following chapter. Nematic liquid crystalline phases are also orientationally tunable with magnetic fields through an analogous mechanism [11].

2.2.2 Substrate Interactions

Liquid crystalline ordering may also be affected, in both degree and direction, through interaction with the substrate molecules comprising a bounding surface. This *anchoring* effect can be induced using a number of distinct techniques to produce several different boundary conditions. In principle many of these mechanisms can be thought of as being similar to, if not intimately linked with, epitaxy exhibited by conventional crystals[20].

As will be seen shortly, it is often advantageous to force the molecular axis to a uniform

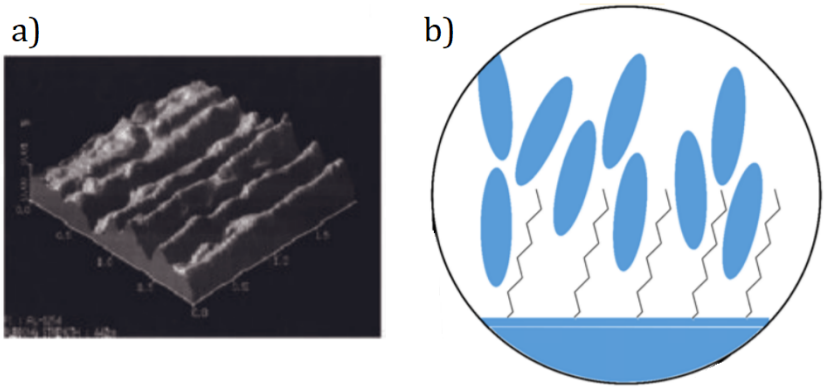

Figure 2.5: a) Micrograph of rubbed polyamide surface used to induce uniform planar anchoring in an LCD cell. From ref [1]. b) Diagram of polymer brush induced homeotropic anchoring. From ref [9].

planar distribution or *planar anchoring*. This is commonly achieved through the use of anchoring compounds, which are rubbed or etched to produce nanometre-scale grooves [1]. These grooves produce an asymmetry in the molecular bonds, and thus the charge, on the surface of the anchoring material which creates a local electromagnetically-induced preference for alignment of the liquid crystal along the grooves [21]. Typical anchoring compounds include polyamides, whose long chain-like structure is amenable to reordering through abrasive rubbing. Anchoring of the molecular orientation of the liquid crystal perpendicular to the plane of the surface or *homeotropic anchoring* is also possible through interaction with elongated surfactant molecules which are themselves homeotropically ordered [9]. These primary methods of creating surface anchoring are depicted in Figure 2.5.

Surface-induced positional anchoring is also possible, and indeed to some finite extent inevitable. As the nematic phase is characterized by translational invariance on macroscopic scales, a surface boundary represents a broken symmetry. The molecular centres of mass will tend to form planes parallel to the surface, however this effect is comparatively weak in contrast to both other surface effects and alignments induced by electric fields [22].

The competition between the ordering induced by surface interactions with that by applied fields, in conjunction with geometric constraints imposed by the topology of the surfaces themselves, is responsible for the highly tunable and specific orientational distributions seen in liquid crystals. Of primary importance to both the theory and implementation of liquid crystal devices is the strength of anchoring at the surface. It is often desirable to

have an anchoring effect at the surface which is dominant to such an extent as to essentially impose a specific degree and direction of ordering regardless of applied fields or bulk considerations. This limit of so-called *strong anchoring* can be determined experimentally using the VanSprang-Yokoyoama technique [23]. Some rubbed polyamide surfactants are capable of inducing sufficiently strong anchoring within the context of the voltages and design parameters of some modern LCD cell technology [7].

2.2.3 Optical

In properly describing the highly structured optical properties liquid crystal phases can produce, it is useful to re-examine the optical properties of conventional crystals as a contrast. It will be seen that the ability of liquid crystals to form manipulatable textures allows them to extend classic crystal optical phenomena into new and exciting properties.

Polarization

Many conventional crystal systems are well known to induce a dephasing effect on electromagnetic waves which pass through them with polarization oblique to the crystal axes. The magnitude of this effect is dependent upon the orientation of the crystal axis relative to the polarization of the incident light [6].

This is an immediate consequence of the dielectric anisotropy of the molecules (which is parlayed into uniform macroscopic dielectric anisotropy by the long-range orientational ordering), to which the speed of propagation in the medium is related as $v = \frac{1}{\sqrt{\epsilon\mu}}$. Thus the components of the electric field along and perpendicular to the molecular axis traverse the medium at different velocities; upon exiting, there will necessarily be a phase difference induced between the two, excepting the case where the phase difference is exactly a multiple of 2π. Therein an initially linearly polarized wave may be dephased into a elliptical polarization of arbitrary eccentricity based on the length of the medium and the magnitude of the dielectric anisotropy.

Rotating linear polarizations without inducing elliptical eccentricity is key to selectively and discretely passing light through crossed polarizers in an optical device. The simplest mechanism to do so can be achieved using homogenous molecular alignments analogous to a crystal and exploiting the degeneracy of the linearity condition. Namely, by setting the incident light polarization to lie at 45° to the parallel and perpendicular molecular axes, the axial components of the electric wave are of equal magnitude. Ensuring a phase retardation of π, the wave remains linearly polarized but is itself rotated by a factor π,

i.e. the wave is moved from an $E_{\parallel} = E_{\perp}$ polarization to an $E_{\parallel} = -E_{\perp}$ polarization. This places a strict value on the depth of the crystalline device relative to the optical anisotropy.

Liquid crystal systems are capable of reproducing this behaviour, and further the presence of spatial variation in the molecular orientation allows for more complicated interactions with light. Uniquely, non-homogenous liquid crystal orientational textures offer the ability to rotate linear polarizations of light continuously by arbitrary degree, using mechanisms requiring shorter depth. *Twisted nematic* phases, also commonly called *cholesteric* phases due to first being observed in plant cholesterols, are defined by a transverse twisting of the molecular orientation shown in Figure 2.6. This helical texture rotates the incident polarization congruent with the molecular axis without inducing elliptical eccentricity and without loss of intensity [1]. This mechanism can be understood rigorously by considering the dispersion relation for an electromagnetic wave passing through two immediate layers which vary in molecular orientation by a small angle [24].

In this way a twisted nematic cell fitted with cross-polarizers allows light to pass through the system without loss. If the surface-induced texture is overridden by a strong applied field as in the ON-state depicted in 2.6, then the light is not rotated and is absorbed by the second polarizer. This is the principle behind the until recently widespread TN-cell LCD. The rate of the polarization rotation relative to the thickness of the material is referred to as the rotary power; liquid crystals exhibit rotary power in the hundreds of revolutions per millimetre. In constrast, rotary power using alternative mechanisms in conventional crystal setups are orders of magnitude lower: quartz gives $\approx 24°/\text{mm}$ [24]. These structures also exhibit a number of other interesting optical properties, including a prospensity to strongly reflect circularly-polarized incident light with opposite-handedness to the helix [1].

Ultimately, cholesteric nematic liquid crystal phases offer the ability to tunably rotate the polarization of light across small distances, making them ideal as waveguides in the selective transmittance of light.

2.2.4 Topological

The freedom of liquid crystals to spatially vary in molecular orientation allows for a sizeable breadth of intimately topologically-rooted phenomena. Of primary interest is the effect of the surface geometry and anchoring on the formation of so-called *textures* and *disclinations*. Nematic texture refers to the vector field of primary molecular alignment; the OFF-state shown in Figure 2.6 is characterized as a 90° twist texture. Disclinations, or nematic defects, represent discontinuities and singularities in the texture and are associated with lowered uniaxial alignment and increased biaxial alignment [1]. Defects can be topologically

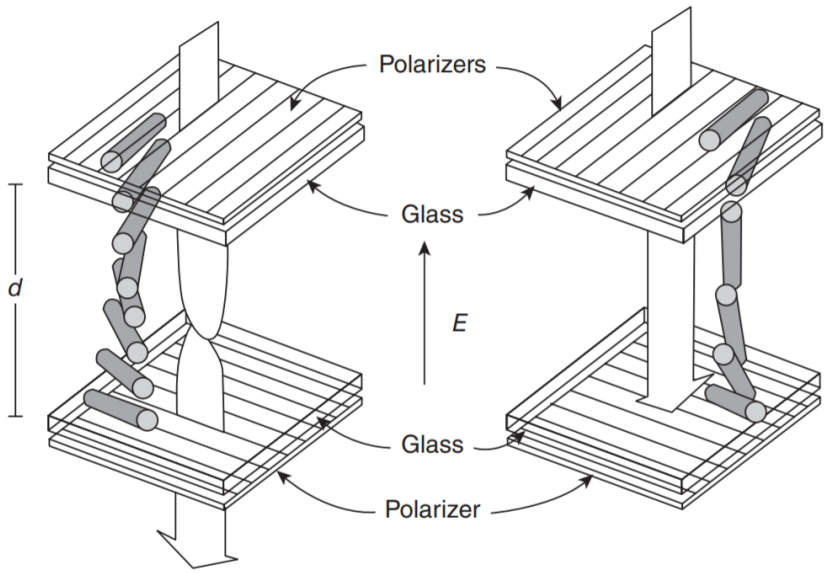

Figure 2.6: Twisted nematic cell ON and OFF states. From ref [1].

required, such as in nematic droplets with homeotropic anchoring [15], or induced by a combination of topology, anchoring, and external fields such as in π-cell LCDs [13]. The study of nematic defects is important to the function of certain liquid crystal devices, though an in-depth discussion of this phenomena is not included here as this work studies exclusively defect-free systems.

2.3 Liquid Crystal Displays

No overview on the practical application of liquid crystal phases could reasonably omit liquid crystal displays (LCDs); these devices represent the primary motivation for the engineering of LC devices and today constitute a multi-billion dollar international industry. Their desired and necessary properties drive the search for new mesogens, engender the structure of standard numerical models, and provide the literature base on which new simulations are commonly validated.

The previously mentioned twisted nematic (TN) cell patented in 1970 represents the first true LCD cell, and became ubiquitous in display technology through the 1980s and 1990s. TN cells benefit from the use of parallel plates to produce the on-state field; not

only is it comparatively easy to manufacture a uniform thin film of sufficiently transparent electrode (typically an indium-tin oxide layer) compared to a discrete patterning, the resulting field is uniform omitting the anistropic effects of the liquid crystal. The primary limitations of the TN cell are a high viewing angle dependency and poor colour reproduction [25]. The discongruity between the ON and OFF state textures complicates design: as rotary power is inversely proportional to twist pitch, there is motivation to apply strong anchoring at the substrates. However, since the ON state must strongly override the helical texture with a uniform one, this necessitates an increase in power drawn by the device to generate the electric field. The OFF state also exhibits competition between the field and the surface anchoring at both boundaries, competition which induces nonuniformity. Even small variations in the OFF state texture can introduce non-zero transmittance, reducing contrast [26] [25].

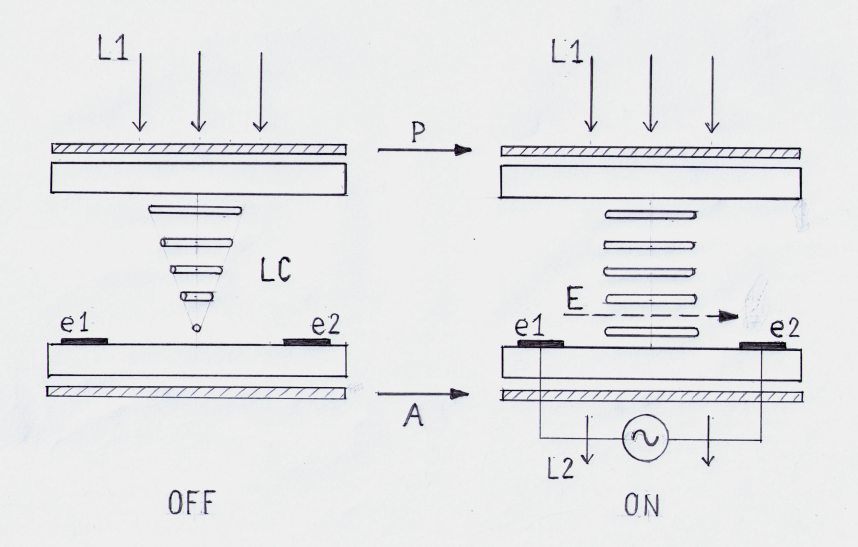

Figure 2.7: Schematic of an in-plane switching mode LCD cell. From ref [10].

A number of LC cell implementations have been developed since the mid 1990s with the goal of supplanting TN and addressing its functional limitations. The number of designs is sizeable, with different incarnations being designed for specific applications and to circumvent patent-protected designs. Currently however, variations on the in-plane switching mode (IPS) cell have become widely adopted. The IPS cell is similar in construction to the TN cell, but it applies a field in the plane of the LC film, shown in Figure 2.7. This patterned electrode configuration is more difficult (and expensive) to manufacture. Additionally, the distance between electrodes must be larger than the thickness of the film to

create a sufficiently horizontal field, increasing the voltage required to match field strength with the TN configuration. However, the incongruity between ON and OFF states is significantly minimized with the applied field acting contrary to the surface anchoring of only one boundary. This lessens the competition between the two mechanisms of control, relaxing the need for a strong applied field and lessening orientational heterogeneity in the ON state. The IPS cell exhibits lower transmittance in the ON state for greater contrast, higher colour fidelity, and significantly wider viewing angle at the cost of higher power draw and longer switching time [1, 27].

Although IPS cells provide a number of attractive optical properties, there remains both numerous permutations of this base principle and alternative LC cells designed to suit a wide range of specific display implementations. The continuous need for the customization of LC cells as well as investigations into their application-specific limitations necessitates the construction of general and rigorous numerical simulations.

Chapter 3

Theory

3.1 Order Parameter Choice, Description, and Properties

Given an understanding of the molecular picture of mesogens, we are free to seek a theory which describes their thermodynamic properties. We require a suitable order parameter associated with the phase, around which expressions for the properties may be constructed.

3.1.1 Scalar Order Parameters and Limitations

In constructing a theory of the free energy of liquid crystals it is sensible to consider the use of a scalar-valued parameter to describe a continuous degree of orientational order. In the simplified case of a purely uniaxial texture, the director constitutes an axis of perfect rotational symmetry about which ordering is a function of only the azimuthal angle θ. Figure 3.2 shows distributions of angular deviation of a uniaxial phase from the director. A continuous measure can be constructed in terms of θ to describe the average magnitude of deviation; as will be seen in the next section, even-numbered Legendre polynomials are a convenient choice. The standard measure, the *scalar order parameter* S, is typically defined as [28]:

$$S = \langle P_2(\theta) \rangle = \frac{3}{2}\langle \cos^2(\theta) \rangle - \frac{1}{2} \tag{3.1}$$

Higher-order even Legendre polynomials are sometimes used to increase accuracy [28]; the headlessness ($\hat{n} = -\hat{n}$) of the director causes the expected value of an odd measure to be zero.

This measure however assumes that the director acts as an axis of rotational symmetry for the angular distribution function. This precludes describing biaxial phases, where a pependicular secondary axis of alignment is present. In biaxial systems, there is no axis where a rotation of any magnitude leaves the system constant. Because of this, scalar order parameter models are inaccurate in describing numerous materials and topologies, and fundamentally incapable of investigating phenomena which arise directly from biaxiality such as trirefringence. They remain popular in literature concerning systems with strong uniaxiality [29, 30, 31, 32, 33].

3.1.2 Frank-Oseen Theory

Putting aside for the moment our reservations about the limitations of a scalar order parameter, we consider a continuum theory for the free energy of a nematic phase developed in 1958 by Frank [4]. Building off of the fundamentals of liquid crystal elasticity theory developed by Oseen in 1920, the *Frank-Oseen* theory expands the free energy density of the system in terms of gradients in the director. Taken to second order these expansion terms are regrouped into four terms representing four fundamental modes of elastic deformation [5]:

$$f_{FO} = \frac{1}{2}k_{11}(\nabla\cdot n)^2+\frac{1}{2}k_{22}(n\cdot\nabla\times n)^2+\frac{1}{2}k_{33}(n\times\nabla\times n)^2-\frac{1}{2}(k_{22}+k_{24})\nabla\cdot(n(\nabla\cdot n)+n\times\nabla\times n) \tag{3.2}$$

where the modes *splay* (k_{11}), *twist* (k_{22}), and *bend* (k_{33}) are depicted in Figure 3.1. The final mode, *saddle-splay* is not easily visualized, and due to its divergence factor is often reformulated to a surface integral via divergence theorem when considering the total free energy off a system. For this reason saddle-splay is sometimes omitted in systems where anchoring effects are strongly dominant at the surface, or the bulk energies dominate [34].

A prime advantage of the Frank-Oseen Theory is that it describes the elastic free energy in terms of these conveniently-interpretable modes, and the constants k_{ii} can be readily measured by examining systems which exhibit only one mode of elastic deformation.

However the Frank-Oseen model is strongly limited by its omission of the following phenomena, many of which are critical to the description of the LC systems we seek to study:

- Biaxial ordering is neglected, as the director only accounts for the primary (uniaxial) alignment

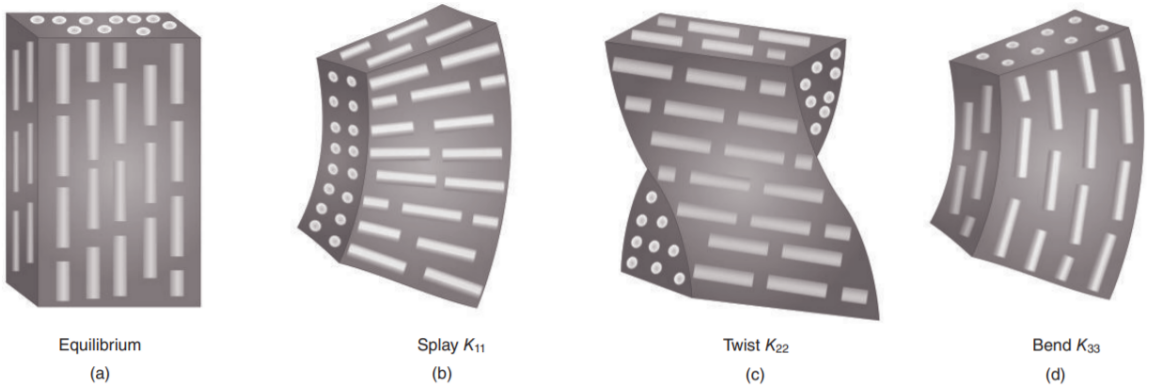

Figure 3.1: Categorization of Frank-Oseen elastic modes. From ref [1].

- Variations in the thermodynamic bulk free energy associated with variation in molecular orientation strength are neglected, i.e. the scalar order parameter S is assumed constant throughout the domain and only the director may vary in the minimization of the free energy.
- Director headlessness is not accounted for, creating large artificial free energy contributions in some texturally complex systems [35].

3.1.3 Alignment Tensor

Modelling LC systems with generality then requires a higher-dimensional order parameter which encapsulates the multiple degrees and directions of ordering LC phases can exhibit. The *alignment tensor* derived by Pierre-Gilles de Gennes provides such an object.

Consider a single LC molecule in the bulk of a material with a molecular axis described by $\hat{u}$, an element of $\mathbf{RP^2}$ which may be thought of as a point on a unit sphere.

A small region of LC material contains some distribution of axes $\vec{u}$ which can be represented as a density function η on the unit sphere $\mathbf{S^2}$. Since there is no meaningful distinction in the choice of $\vec{u}$ or $-\vec{u}$ to describe the molecular axis, the distribution is constant across antipodes ($\eta(a) = \eta(-a), a \in \mathbf{S^2}$). In the thermodynamic limit the distribution is

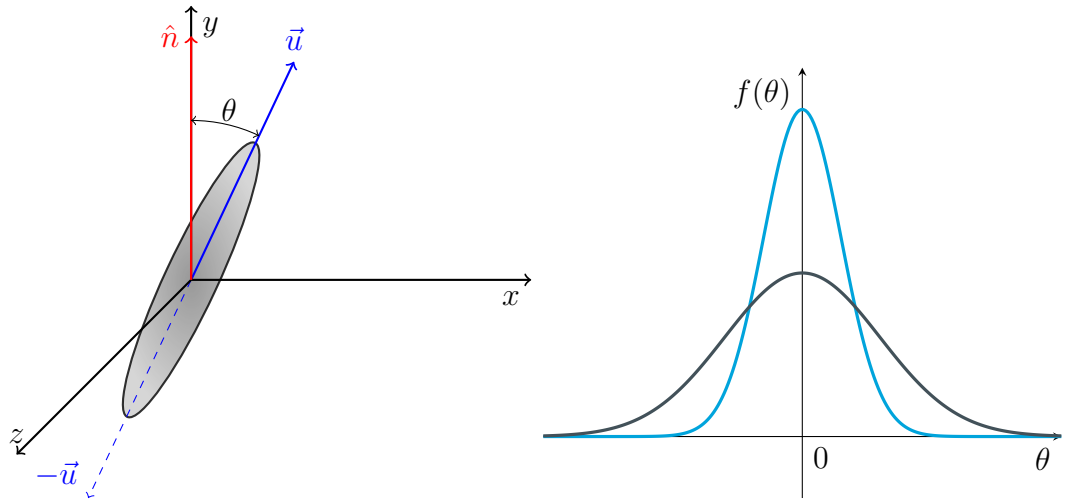

Figure 3.2: a) Schematic of molecular orientation, where $\hat{n}$ is the director and $\hat{u}$ is a particular molecular axis. b) Uniaxial orientation distributions corresponding to low (black) and high (cyan) degrees of ordering

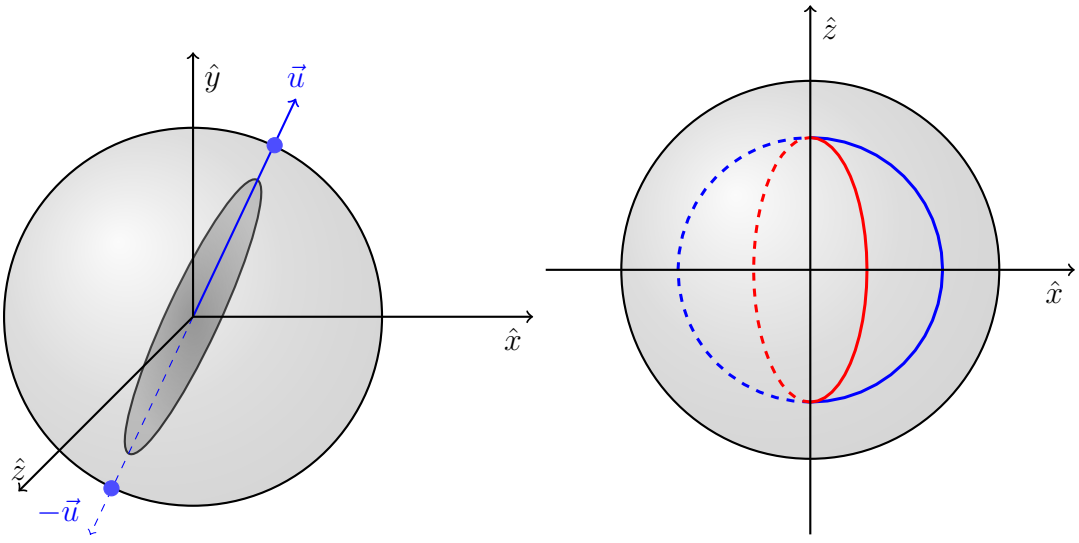

Figure 3.3: a) Molecular axis and corresponding spaces on unit sphere b) Lines of constant probability density for a uniaxial (blue) and biaxial (red) phases with secondary axis $\hat{z}$

continuous, and we can examine the tensorial moments thusly:

$$\int_{\mathbf{S^2}} \mathbf{u}\,\eta(\mathbf{u})d\mathbf{S} = 0 \qquad \text{First Moment} \tag{3.3}$$

$$\int_{\mathbf{S^2}} \mathbf{u}\otimes\mathbf{u}\,\eta(\mathbf{u})d\mathbf{S} \equiv \mathbf{M} \qquad \text{Second Moment} \tag{3.4}$$

The first moment is trivially zero by the antipodal property. The second moment however, forms a symmetric matrix $\mathbf{M}$. When the LC molecules are in the isotropic phase, $\eta(\mathbf{u})$ is constant and thus

$$\mathbf{M}_{iso} \equiv \int_{\mathbf{S^2}} \mathbf{u}\otimes\mathbf{u}\,\frac{1}{4\pi}d\mathbf{S} \tag{3.5}$$

$$= \frac{1}{4\pi}\int_{\mathbf{S^2}} \begin{bmatrix} u_1u_1 & u_1u_2 & u_1u_3 \\ u_2u_1 & u_2u_2 & u_2u_3 \\ u_3u_1 & u_3u_2 & u_3u_3 \end{bmatrix} d\mathbf{S} \tag{3.6}$$

$$= \frac{1}{3}\mathbf{I} \tag{3.7}$$

where $\mathbf{I}$ is the identity matrix. The de Gennes *alignment tensor* is then defined as the deviation of $\mathbf{M}$ from the isotropic value; this sets the order parameter to the zero matrix at the phase transition and is then congruent with Landau expansions of thermodynamic quantities [28].

$$\mathbf{Q} \equiv \mathbf{M} - \mathbf{M}_{iso} = \int_{\mathbf{S^2}} (\mathbf{u}\otimes\mathbf{u} - \frac{1}{3}\mathbf{I})\,\eta(\mathbf{u})d\mathbf{S} \tag{3.8}$$

$\mathbf{Q}$ is symmetric and traceless, i.e. $\mathbf{Q} = \mathbf{Q^T}$, $Tr(\mathbf{Q}) = 0$. These four constraints reduce the number of degrees of freedom from nine to five. This is reflective of the number of independent values needed to specify the vectors representing uni- and bi-axiality: a system of two vectors in three dimensions constrained by mutual orthogonality similarly has (6-1=5) degrees of freedom. Because $\mathbf{Q}$ is real and symmetric, its eigenvectors $\mathbf{n}, \mathbf{m}, \mathbf{l}$ form an orthonormal basis in which Q may be diagonalized:

$$\mathbf{Q} = \lambda_1\mathbf{n}\otimes\mathbf{n} + \lambda_2\mathbf{m}\otimes\mathbf{m} + \lambda_3\mathbf{l}\otimes\mathbf{l} \tag{3.9}$$

$\mathbf{Q}$ can then be re-expressed in a form that more clearly identifies the degrees of uniaxial and biaxial ordering:

$$\mathbf{Q} = S(\mathbf{n}\otimes\mathbf{n} - \frac{1}{3}\mathbf{I}) + P(\mathbf{m}\otimes\mathbf{m} - \mathbf{l}\otimes\mathbf{l}) \tag{3.10}$$

where $S = \frac{3}{2}\lambda_1$ is a scalar measure of the degree of uniaxial alignment along the director $\mathbf{n}$, and $P = \frac{\lambda_2 - \lambda_3}{2}$ is a scalar measure of the degree of biaxial alignment along the secondary axis $\mathbf{m}$. From (3.8) it can be seen that $-\frac{1}{3} \leq \lambda_i \leq \frac{2}{3}$ and thus $-\frac{1}{2} \leq S \leq 1$. To interpret the meaning and range of S, we can consider the uniaxial case where $P = 0$ and compare expressions between the diagonalized and distributional forms [28]:

$$\mathbf{nQn} = S\mathbf{n}(\mathbf{n} \otimes \mathbf{n} - \frac{1}{3}\mathbf{I})\mathbf{n} \tag{3.11}$$

$$= S(\mathbf{n}(\mathbf{n} \otimes \mathbf{n})\mathbf{n} - \frac{1}{3}\mathbf{nIn}) \tag{3.12}$$

$$= \frac{2}{3}S \tag{3.13}$$

$$\mathbf{nQn} = \int_{\mathbf{S^2}} \mathbf{n}(\mathbf{u} \otimes \mathbf{u} \ - \frac{1}{3}\mathbf{I})\ \mathbf{n}\ \eta(\mathbf{u}) d\mathbf{S} \tag{3.14}$$

$$= \langle \mathbf{n}(\mathbf{u} \otimes \mathbf{u})\mathbf{n} - \frac{1}{3}\mathbf{nIn} \rangle \tag{3.15}$$

$$= \langle (\mathbf{n} \cdot \mathbf{u})^2 - \frac{1}{3} \rangle \tag{3.16}$$

$$= \langle \cos^2\theta \rangle - \frac{1}{3} \tag{3.17}$$

Where θ is the angle between the director and molecular axis. Thus combining eqns (3.13) and (3.17):

$$S = \frac{3}{2}\langle \cos^2\theta \rangle - \frac{1}{2} \tag{3.18}$$

which identifies S as the expectation value of the second Legendre polynomial in terms of $\cos\theta$. Thus the alignment tensor recovers the scalar order parameter from uniaxial theory, while also providing a similar measure of biaxiality. As cosine ranges from -1 to 1 we again recover that $-\frac{1}{2} \leq S \leq 1$, though now it can be seen that negative values of S are of questionable physicality. Considering $S = -\frac{1}{2}$, we have that the molecular axes *all* lie perpendicular to the director, which is not self-consistent. Indeed, $S < 0$ corresponds to geometrically allowable but ultimately highly unstable distributions, while $S = 0$ corresponds to the isotropic phase. $0 < S \leq 1$ corresponds to increasing strength of uniaxial ordering.

3.2 Landau-de Gennes Free Energy Model

3.2.1 Bulk Free Energy

Armed with an order parameter which properly encodes multiple modes of ordering, a phenomenological expression for the free energy density can be obtained as a Landau expansion of (rotationally invariant) combinations of Q and its gradients. Taken to fourth order, the non-gradient terms form an expression for the bulk free energy density: the energy associated with with the nematic-isotropic phase transition [5].

$$f_b = f_{iso} + \frac{1}{2}a_0(T - T_{ni})Q_{ij}Q_{ji} - \frac{1}{3}b\,Q_{ij}Q_{jk}Q_{ki} + \frac{1}{4}c\,(Q_{ij}Q_{ji})^2 + \mathcal{O}(Q^5) \tag{3.19}$$

The constants a_0, b, and c are experimentally-obtained temperature-independent parameters associated with the specific liquid crystal species. T^*_{ni} is the supercooling temperature, the temperature at which the isotropic phase is no longer metastable; this is slightly below the transition temperature T_{ni}. By convention, the sign of the third order term is negative in order to keep all phenomenological constants positive. Because only the minimization of the free energy is relevant to modelling the dynamics of the system, the constant free energy of the isotropic phase f_{iso} is hereon omitted.

3.2.2 Elastic Free Energy

The gradient terms of the Landau expansion represent energy associated with elastic deformation of the phase. These terms can be interpreted as penalizing combinations of different gradients of the director within the material [3, 13].

$$f_{elas} = \frac{1}{2}L_1(\partial_i Q_{jk}\partial_i Q_{kj}) + \frac{1}{2}L_2(\partial_i Q_{ij}\partial_k Q_{kj}) + \frac{1}{2}L_3(Q_{ij}\partial_i Q_{kl}\partial_j Q_{kl}) + \frac{1}{2}L_{24}(\partial_k Q_{ij}\partial_j Q_{ik}) + \mathcal{O}([\nabla Q]^3) \tag{3.20}$$

It is important to note that these alignment tensor elastic constants are not analogous to the elastic constants of the uniaxial Frank-Oseen model; whereas the Frank-Oseen constants can be seen as individually penalizing splay, twist, bend, and saddle-splay deformations, the the Landau-de Gennes elastic constants have no simple physical interpretation.

The common *single constant* approximation:

$$L_1 \neq 0,\ L_2 = L_3 = L_{24} = 0 \tag{3.21}$$

has the effect of penalizing all modes of deformation identically with the exception of saddle-splay, which is negated. In practice, thermotropic liquid crystals can vary significantly in the free energy penalties of the elastic modes [7].

Unlike the Frank-Oseen model, wherein the elastic parameters are easily measured through the Fréedericksz transition, there is no simple experimental procedure to determine the Landua-de Gennes constants; since the Landau-de Gennes model is a strict generalization of the Frank-Oseen model the constants are here instead derived by equating the two models under the latter's assumptions. That is, assuming purely uniaxial alignment and a constant degree of uniaxial ordering throughout the system, the two models are equivalent leading to the relations [13]:

$$L_1 = \frac{1}{6S_{eq}^2}(k_{33} - k_{11} + 3k_{22}) \tag{3.22}$$

$$L_2 = \frac{1}{S_{eq}^2}(k_{11} - k_{22} - k_{24}) \tag{3.23}$$

$$L_3 = \frac{1}{2S_{eq}^3}(k_{33} - k_{11}) \tag{3.24}$$

$$L_{24} = \frac{1}{S_{eq}^2}k_{24} \tag{3.25}$$

$$\tag{3.26}$$

where S_{eq} is the equilibrium uniaxial order parameter under the same assumptions, given by considering the uniaxial bulk free energy [3]:

$$f_{bulk}(S) = \frac{1}{3}a_0(T - T_{ni}^*)S^2 + \frac{2}{27}bS^3 + \frac{1}{9}cS^4 \tag{3.27}$$

whose minimization gives:

$$S_{eq} = \frac{b}{4c}\Big(1 + \sqrt{1 - 24\frac{(a_0c(T - T_{ni}^*))}{b^2}}\Big) \tag{3.28}$$

It is perhaps somewhat unfortunate that an approximation of low biaxiality must be used here to obtain elastic parameter values, given the ability to describe biaxiality being one of the major incentives of using a tensorial order parameter. For this reason we must still remain cognizant of significant spatial variation in the uniaxial order parameter S in simulation and the impact it has on the precision of the model's elastic free energy.

3.2.3 Electric Free Energy

Seeking to quantify the interaction of the phase with an external field, we have the standard expression for the electric energy associated with an applied field

$$f_{elec} = \frac{1}{2}(D \cdot E) \tag{3.29}$$

For a dielectrically anistropic material, the displacement field is related to the electric field via the dielectric tensor:

$$D_i = \epsilon_{ij} E_j \tag{3.30}$$

The dielectric tensor itself is dependent on the orientation of the LC molecules, and thus its expression must be a function of Q. Isolating this dependence, it can be written as a sum of the average (isotropic) permittivity and the anisotropy [30]:

$$\epsilon_{ij} = \epsilon_{iso}\,\delta_{ij} + \Delta\epsilon\,Q_{ij} = \frac{\epsilon_\parallel + 2\epsilon_\perp}{3}\delta_{ij} + (\epsilon_\parallel - \epsilon_\perp)\,Q_{ij} \tag{3.31}$$

Thus the electric free energy density of the liquid crystal is

$$f_{elec} = \frac{\epsilon_0}{2}\Big(\frac{\epsilon_\parallel + 2\epsilon_\perp}{3}\delta_{ij} + (\epsilon_\parallel - \epsilon_\perp)Q_{ij}\Big)E_i E_j \tag{3.32}$$

Since the isotropic term is spatially invariant, the sign of the dielectric anisotropy determines whether this free energy is minimized by alignment along or counter to the applied field. There exists a similar term describing interaction with an applied magnetic field; however in this work we will only apply external electric fields [11].

3.2.4 Surface Interaction Free Energy

The free energy associated with the surface interaction is taken as the Rapini-Papoular model, which simply penalizes deviation from the preferred ordering induced by the substrate:

$$f_s = \frac{1}{2}\alpha(Q_{ij} - Q^s_{ij})^2 \tag{3.33}$$

where Q^s is the alignment tensor associated with the surface at equilibrium, and α is an experimentally-obtained parameter.

In principle, a more general expression may be obtained similarly to the bulk and elastic free energies; that is, by expanding in terms of the alignment tensor and the surface normal

and keeping rotationally invariant terms. Assuming a uniform and weakly-penetrating surface interaction (confining the effect to the first few layers of the nematic)[36]:

$$f_s = f_{iso} + \alpha_{11} k_1 Q_{ij} k_j + \alpha_{21} k_i Q_{ij} Q_{jl} k_l + \alpha_{22} (k_i Q_{ij} k_j)^2 + \mathcal{O}(Q^3) \tag{3.34}$$

This formulation has the benefit over Rapini-Papoular of being capable of encapsulating planar degenerate ordering, i.e. where the surface induces planar anchoring but with no preferred direction. Varying the parameters α_{ij} amounts to varying both the strength of surface anchoring and the preferred alignment (homeotropic or planar).

However, to remain accurate away from the transition temperature, this expression would need to be expanded to higher order, with each order having multiple terms. This introduces a sizeable new non-trivial set of phenomenological parameters whose values and temperature dependence would need to be experimentally measured for any given surfactant, and possibly for surfactant-mesogen combinations. Since we wish to simulate well into the nematic phase, we instead implement Rapini-Papoular anchoring.

Total Free Energy

Combining and integrating over all contributions, we arrive at the total free energy of the liquid crystal system:

$$F = \iiint_\Omega \underbrace{f_{bulk} + f_{elas} + f_{elec}}_{f_v} \, d\Omega + \iint_A f_s \, dA \tag{3.35}$$

$$\begin{aligned} &= \iiint_\Omega \Bigg(\frac{1}{2} a_0 (T - T_{ni}) Q_{ij} Q_{ji} - \frac{1}{3} b \, Q_{ij} Q_{jk} Q_{ki} + \frac{1}{4} c \, (Q_{ij} Q_{jk})^2 \\ &+ \frac{1}{2} L_1 (\partial_i Q_{jk} \partial_i Q_{kj}) + \frac{1}{2} L_2 (\partial_i Q_{ij} \partial_k Q_{kj}) + \frac{1}{2} L_3 (Q_{ij} \partial_i Q_{kl} \partial_j Q_{kl}) + \frac{1}{2} L_4 (\partial_k Q_{ij} \partial_j Q_{ik}) \\ &+ \frac{\epsilon_0}{2} \Big(\frac{\epsilon_\parallel + 2\epsilon_\perp}{3} \delta_{ij} + (\epsilon_\parallel - \epsilon_\perp) Q_{ij} \Big) \partial_i V \partial_j V \Bigg) \, d\Omega + \iint_A \frac{1}{2} \alpha (Q_{ij} - Q^s_{ij})^2 \, dA \end{aligned} \tag{3.36}$$

where we have chosen to work in terms of the electric potential field V.

3.3 Gauss's Law for Dielectrically Anisotropic Mediums

As discussed earlier we must also solve for the electric potential field inside the system. This is given by the macroscopic formulation of Gauss's law as:

$$\partial_i D_i = \rho_f \tag{3.37}$$

For a dielectrically anisotropic medium, the displacement field is related to the potential field through the dielectric *tensor* [13] [37]:

$$\partial_i \epsilon_{ij} \partial_j V = 0 \tag{3.38}$$

which as previously, is a function of the molecular alignment through the alignment tensor, giving:

$$\partial_i \Big(\frac{\epsilon_\parallel + 2\epsilon_\perp}{3} \delta_{ij} + (\epsilon_\parallel - \epsilon_\perp) Q_{ij} \Big) \partial_j V = 0 \tag{3.39}$$

3.4 Fréedericksz Transition

A key phenomena, both for determining the value of mesogen elastic constants and validating a model, is the Fréedericksz transition. In a nematic liquid crystal system with non-zero anchoring energy in the absence of an external field, the equilibrium texture will be governed by the surface interaction. As an external field is switched on such that its preferred orientation is counter to that of the surfaces, the texture becomes characterized by the competition between the electric and elastic free energies. At small values of electric field strength, it is not favourable for the texture to realign with the field to any degree; only after a critical field strength is reached will the molecular orientation then begin to continuously deform from the initial state [1, 25].

This phase transition can be observed experimentally to compare the relative values of the electric and elastic free energies. In a Fréedericksz cell configuration, it is possible to isolate the contribution of an individual elastic mode. We present here the typical derivation of this effect within Frank-Oseen theory with respect to the K_{22} twist constant.

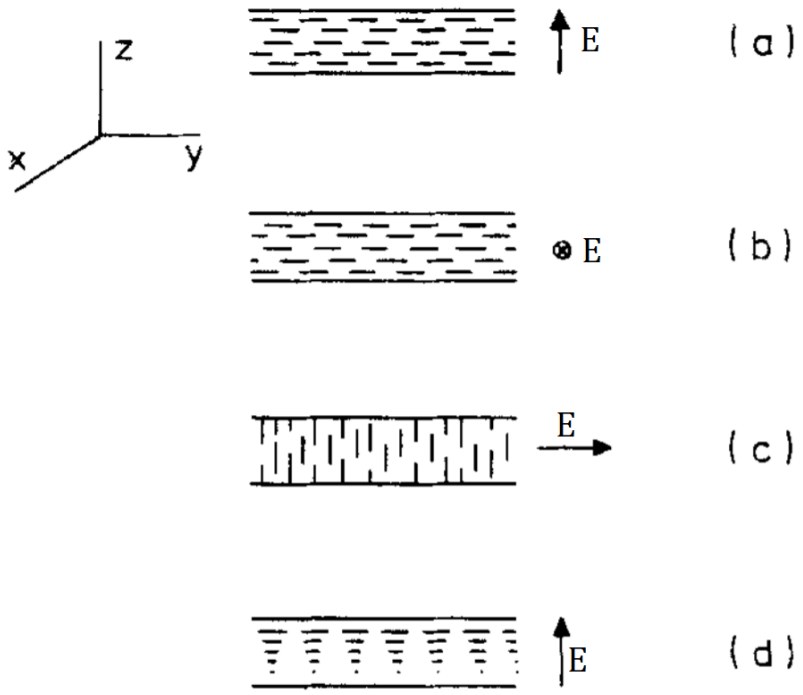

Figure 3.4: Various configurations for the Fréedericksz transition. Adapted from ref [11].

Consider a nematic liquid crystal thin film with planar anchoring in the $\hat{y}$ direction on the $\hat{z}$ boundaries, as depicted in Figure 3.4 b). Application of an electric field in the $\hat{x}$ direction causes spatial variation in the director field; this pure splay deformation produces a director of varying alignment:

$$\hat{n} = \cos(\theta(z))\hat{y} + \sin(\theta(z))\hat{x} \tag{3.40}$$

Assuming uniaxiality and constant S, we apply the Frank-Oseen model for elastic deformation energies. At the point of transition the energy contribution of the non-twist modes is negligible, and the energy associated with deformation is then [1]:

$$U = U_{elas} + U_{elec} = \frac{1}{2}K_{22}\Big(\frac{\partial\theta}{\partial z}\Big)^2 - \frac{1}{2}\epsilon_0\Delta\epsilon E^2\sin^2(\theta) \tag{3.41}$$

Minimizing this using the calculus of variations gives the Euler-Lagrange equation:

$$\frac{\partial U}{\partial\theta} - \frac{d}{dz}\Big(\frac{\partial U}{\partial\frac{d\theta}{dz}}\Big) = 0 \rightarrow K_{22}\frac{d^2\theta}{dz^2} + \epsilon_0\Delta\epsilon E^2\sin\theta\cos\theta = 0 \tag{3.42}$$

For a cell of thickness d, there is a critical electric field value E_c

$$E_c = \frac{\pi}{d}\sqrt{\frac{K_{22}}{\epsilon_0\Delta\epsilon}} \tag{3.43}$$

below which the functional (3.42) is minimized by a constant $\theta = 0$ function. Thus the nematic texture of the cell exhibits no response to an external field lower than this critical threshold. Above E_c, (3.42) is minimized by a nonconstant θ function; under this field the nematic texture will deform as it becomes energetically favourable to align with the external field to some degree [1].

By measuring the deformation of the cell (commonly through measurements of the capacitance or optical transmittance [7]) in response to a continuously increasing applied field, it is possible to determine E_c and calculate K_{11}. The same process can be applied to other cell/field combinations which induce exclusively bend or twist deformation to obtain the other Frank constants. All other single-mode cells depicted in Figure 3.4 follow an analogous derivation, and thus the generalized form of equation (3.43) is simply:

$$E_c = \frac{\pi}{d}\sqrt{\frac{K_{ii}}{\epsilon_0\Delta\epsilon}} \tag{3.44}$$

This methodology requires highly controlled experimental parameters in order to ensure the isolation of a single elastic mode at the point of transition. The isolation of the splay

mode relies on an assumption of strong surface anchoring (i.e. $\alpha \to \infty$), and even small extraplanar deviations in the director at the surface produce significant changes in the critical voltage [38]. Additionally even comparatively small deviations in the direction of the applied field also impact the transition phenomena. This lends difficulty to generating the necessary transverse fields for the bend and twist cell geometries, which require uniform fields in the plane of the film. For this reason, in practice Fréedericksz transition methods often instead use a variety of textural configurations with known mode ratios (i.e. the free energy contribution of each mode is known) and solve the resulting system of equations for the K_{ii} constants [7] [39].

3.5 Numerical Methods

3.5.1 Free Energy Minimization

Given a formulation 3.36 for the total free energy of the system, the equilibrium state can be obtained by solving for the minimization in terms of the order parameter Q and electric potential V, satisfying an appropriate set of boundary conditions. A standard variational approach results in the Euler-Lagrange equation [1] [15]:

$$\frac{\partial f_v}{\partial Q} - \nabla \cdot \frac{\partial f_v}{\partial \nabla Q} = 0 \tag{3.45}$$

with boundary condition:

$$\frac{\partial f_s}{\partial Q} - k \cdot \frac{\partial f_s}{\partial \nabla Q} = 0 \tag{3.46}$$

3.5.2 Finite Element Implementation

A time-perturbation numerical method is used to solve the Euler-Lagrance equations: 3.45 is modified with a time derivative term:

$$\frac{\partial f_v}{\partial Q} - \nabla \cdot \frac{\partial f_v}{\partial \nabla Q} = \mu \frac{\partial Q}{\partial t} \tag{3.47}$$

[1] This model equation was originated by Fred Fu.

where μ is a rotational viscosity of the phase. This formulation allows for an initial condition significantly different from the equilibrium solution to be used, time-stepping forward without requiring significant foreknowledge of the steady state [40].

A finite element scheme is implemented to solve the system of partial differential equations 3.47 and 3.39; finite element schemes are particularly well suited for simulating complicated domains and allow for highly irregular and even unstructured meshes. FE schemes exhibit high accuracy in problems involving complicated boundary conditions, and are thus useful in simulating arbitrary configurations of nematic cells [41]. The implemented scheme is a continuous Galerkin method using first-order Lagrange interpolants as the test functions.

Equations 3.47 and 3.39 combined are initially rewritten in the weak form - multiplying through by a weighting function v and integrating over the domain gives [2] [15]:

$$\begin{aligned}\iiint_\Omega \mu_r \frac{\partial Q_{ij}}{\partial t} v_{ji} d\Omega + \iiint_\Omega \Big[\Big(aQ_{ij} - b(Q_{ik}Q_{kj} - \frac{1}{3}Q_{kl}Q_{lk}\delta_{ij}) + c(Q_{kl}Q_{lk}Q_{ij}) \\ - \frac{\epsilon_0}{2}(\Delta\epsilon)(\partial_i V \partial_j V - \frac{1}{3}\partial_k V \partial_k V \delta_{ij}) \Big) v_{ji} + L_1(\partial_k Q_{ij} \partial_k v_{ji}) \\ + (L_2 + L_{24}) \Big(\frac{1}{2}(\partial_i Q_{kj} \partial_k v_{ji} + \partial j Q_{ki} \partial_k v_{ji}) - \frac{1}{3}\partial_l Q_{lk} \partial_k v_{ji} \delta_{ij} \Big) \\ + L_3 \Big(Q_{kl} \partial_l Q_{ij} \partial_k v_{ji} + \frac{1}{2}\partial_i Q_{kl} \partial_j Q_{kl} v_{ij} - \frac{1}{6}\partial_k Q_{lm} \partial_k Q_{lm} \delta_{ij} v_{ji} \Big) \\ + \Big(\Big(\frac{\epsilon_\parallel + 2\epsilon_\perp}{3}\delta_{ij} + (\Delta\epsilon) Q_{ij} \Big) \partial_j V \Big) \partial_i v \Big] d\Omega + \iint_S \alpha v_{ji} dS = 0 \end{aligned} \quad (3.48)$$

The system domain is then discretized into a set of tetrahedral subdomain elements. On each element, the numerical solution is represented by a combination of basis functions; here we use linear Lagrange interpolants. In this way the solution is discretized to a finite number of degrees of freedom. Substituting this into the weak form (3.48) results in a system of nonlinear ordinary differential equations, which are solved simulatenously via Newton's method.

Given the long variation in timescales found in the relaxational dynamics of nematic liquid crystal systems, an adaptive timestepping system is implemented. At each iteration in time, the solution $Q_{t+\Delta t}$ is computed twice: first using a single Δt timestep, and again using two $\frac{\Delta t}{2}$ timesteps. The local error at this step is taken as the difference in these

[2] The Landau-de Gennes portion of the weak form was originated by Fred Fu.

two solutions: if the local error is higher than a user-defined tolerance then the timestep is decreased proportionally and the process repeated until sufficiently small local error is predicted[15].

The finite element implementation used in this thesis including the above described adaptive timestepping is built off of a comprehensive existing implementation for uncoupled, single-boundary simulations in uniform electric fields by Fred Fu, whose contributions cannot be neglected [15].

3.5.3 Weak Form - Gauss's Law

Presented here is the derivation of the weak form of the macroscopic formulation of Gauss's Law. Beginning with the expression:

$$\partial_i D_i = \rho_f = 0 \tag{3.49}$$

Obtaining the weak formulation by integration and the addition of the test function ν

$$\iiint_\Omega \Big(\partial_i D_i\Big)\nu d\Omega = 0 \tag{3.50}$$

Using product rule

$$\iiint_\Omega \Big[\partial_i\Big(D_i\nu\Big) - D_i\partial_i\nu\Big] d\Omega = 0 \tag{3.51}$$

Applying divergence theorem

$$\oint_A n_i D_i \nu \, dA - \int_\Omega D_i \partial_i \nu \, d\Omega = 0 \tag{3.52}$$

Re-expressing in terms of the electric potential and dielectric tensor

$$\oint_A n_i \epsilon_{ij} \partial_j V \nu \, dA - \int_\Omega \epsilon_{ij} \partial_j V \partial_i \nu \, d\Omega = 0 \tag{3.53}$$

3.6 Previous Work in Thermotropic Nematic Liquid Crystal Simulation

To place new simulations of liquid crystal display cells in a meaningful context, and moreso to interpret their results properly in a way that is conductive to further work and refinement, it is necessary to underline both the historical and contemporary bodies of work in this field.

One of the first theoretical models for the nematic LC phase is the Frank-Oseen model [4], which characterizes the free energy of the system in terms of four modes of director distortion. This fundamentally hydrostatic formulation was further developed by Ericksen in 1961 [42] and Leslie in 1968 [43] to create the dynamic Ericksen-Leslie theory. Ericksen-Leslie was used in some of the first numerical simulations of liquid crystal display cells in the 1970s; simulations of the then-dominant twisted-nematic design exhibited general transmission phenomena agreement with experiment [12] [44]. Notably, less well understood behaviour such as the tendency of a TN cell to have a non-monotonically decreasing transmission curve (a so-called 'bounce') between the ON- to OFF-states as in Figure 3.5, was recovered and explained, in this case as arising from a particular dynamical structure in the bulk of the cell [12].

As discussed the Frank-Oseen formulation relies on several approximations, most notably the assumptions of purely uniaxial ordering with uniform degree and an inability to acknowledge the headlessness of the director. Kilian and Hess introduced a numerical formulation of single-constant Frank-Oseen theory which used a tensorial formulation of the director to preserve the symmetry properties of the texture, i.e. $(\hat{n} = -\hat{n})$ [35]. This prevented the accidental inclusion of 'phantom' free energy contributions arising in the simulation of texturally complex domains. They showed reasonable agreement with this formulation and experiment regarding the Fréedericksz transition threshold and reorientation timescales, however the description of orientational defects was at best qualitative [45]. Simulations of the transmittance profiles and contrast ratios of In-Plane Switching LCD cells using this numerical approach reported agreement with experiment to within 10% [46].

Although Ericksen-Leslie improved upon Frank-Oseen by allowing the degree of uniaxial ordering to vary spatially, neither model offers a formalism for describing biaxial ordering within nematic phases. Numerical simulation using the Landau-de Gennes model, which constitutes the most general continuum theory for nematic liquid crystals [47], makes use of a higher-order order-parameter to encode biaxiality. Such a theory is necessary for the numerical simulation of LCD cell designs which inherently involve defect structures. Mori et al. showed that in π-cells, which exhibit topologically-demanded defects, Frank-Oseen theory was unable to predict the equilibrium texture, again producing phantom free energies due to director symmetries in the defect regime. However, an analagous Landau-de Gennes implementation sufficiently matched experimental values of the texture, especially with respect to the defects as shown in Figure 3.5 [13].

Within works using all of the above theories, there exists a broad range of implementations of external electric fields. It is common to assume an equilibrium or transient field, which is then used as a constant model parameter [48, 12, 44, 33]. These assumptions omit

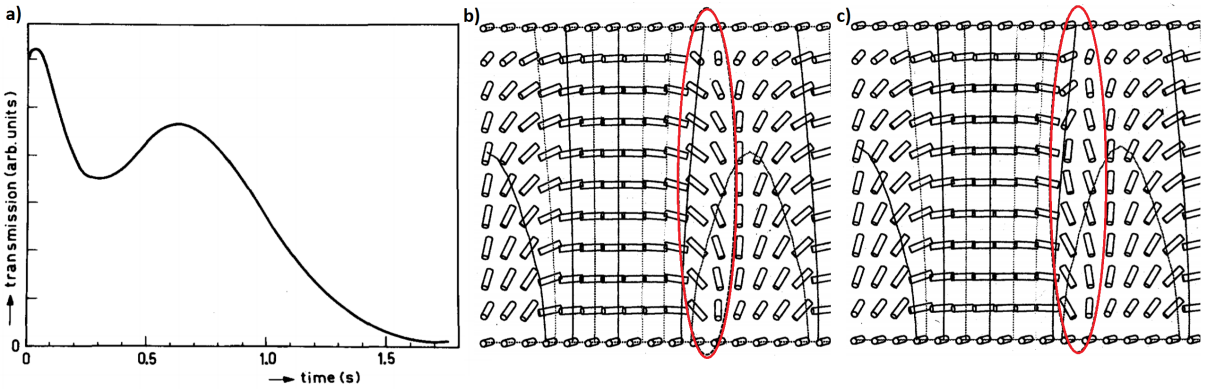

Figure 3.5: a) The transmission 'bounce' observed in TN-cell LCDs, from ref [12]. Splay/bend mode defect line (highlighted in red) as predicted b) correctly through the Landau-de Gennes model and c) incorrectly through the Frank-Oseen model. Adapted from ref [13].

the coupling effect which takes place in liquid crystal systems: as the director reorients in the presence of an external field, the dielectric properties of the phase change, affecting the net field within the material. Especially in domains where there exists no obvious equilibrium field to impose, some studies handle this coupling appropriately by simultaneously or iteratively solving Gauss's law alongside the free energy minimization [37, 30, 13, 46, 32].

The further development of liquid crystal theory is significantly driven by industrial interest in LC applications, most notably of course LCD technologies. New interactions are added to existing models through the inclusion of additional free energies, themselves often necessitated by the consideration of new mesogenic species. Recently Kim et al. introduced a term in the Frank-Oseen model corresponding to the flexoelectric effect, which couples the geometric deformation of the director field to the molecular polarization, studying the effects within the context of In-Plane Switching mode LCD cells [29]. The inclusion of this consideration predicted a change in cell transmittance associated with constructive or deconstructive interaction of the applied field with the flexoelectric polarization, demonstrating not only the complexity of liquid crystal systems but that there is still a great amount of work to be done in fully describing them.

Ultimately, contemporary work makes use of all three continuum theories (Frank-Oseen, Ericksen-Leslie, Landau-de Gennes) under a sizeable variety of approximations and assumptions. Historically, the primary goal of simulation has been to discover and understand liquid crystalline phenomena; as high-fidelity numerical simulation increasingly accentuates or supplants physical experimentation in the practical engineering of liquid

crystalline devices, we seek a stronger understanding of model precision. To that end, we are interesting in comparative study of models using different assumptions.

In this work we implement the most general Landau-de Gennes theory with non-equal elastic parameters, with appropriate coupling between the external field and molecular orientation. Numerical simulations of the Fréedericksz transition and in-plane switching LCD cells are performed to study and contextualize the model precision. Uncoupled simulations using the most accurate ad-hoc approximations for the electric field are compared against in order to understand the significance of coupling and the specific dynamical structures omitted by simpler models in LCD systems.

Chapter 4

Simulation of Single Elastic Mode Cells

4.1 Overview

In order to both validate the implemented continuum model and investigate the dynamics associated with coupling between molecular orientation and external fields, a study of liquid crystalline thin films was performed.

New mesogenic species are commonly engineered from their well-understood chemical building blocks to suit an application, and existing species are occasionally lifted from relative obscurity for similar purposes. Accurate studies of their numerous elastic, thermodynamic, and electrical parameters require precise experimental method, and the precision of these measurements is often difficult to quantify. Table 4.1 holds a number of reported values for the dielectric constants of 4-Cyano-4'-pentylbiphenyl (5CB), a room temperature nematic liquid crystal with broad application. It is then of practical importance to understand the impact of parameter variance on the dynamics predicted by the model.

The model and parameter derivations also make use of several approximations. Although the alignment tensor is able to encapsulate biaxial ordering, the Landau-de Gennes elastic constants are derived from the Frank-Oseen constants under the assumption of trivial biaxiality, which motivates a strong understanding of biaxiality within simulated domains.

Given a validated model which sufficiently matches experimental observations, we then seek to study the impact of solving Gauss's law simultaneous to the free energy minimiza-

$\epsilon_\perp(\Delta T = 10°)$	$\epsilon_\parallel(\Delta T = 10°)$	$\epsilon_{iso}(\Delta T = 3°)$	Source
6.85	18.4	11.0	[49]
6.35	17.6	10.6	[50]
7.7	20.2	11.8	[51]
6.8	19.5	11.2	[52]
6.6	17.7	11.2	[53]
6.5	18.4	11.3	[54]
6.6	19.7	11.2	[7]

Table 4.1: Reported values of perpendicular, parallel, and isotropic dielectric constants of 5CB. Adapted directly from [7].

tion by comparing our model to the common linear approximation to the potential field. Quantifying variation in the electric field for a topologically simple texture such as the one discussed in this chapter serves as a useful reference when examining the much more complicated textures of later simulations.

The specific goals of this section are as follows:

- Validate the implemented model through comparison to experimental observations of the Fréedericksz transition. Perturb the model parameters within their experimentally reported ranges to quantify the precision of the model and understand any discrepancy with experiment.
- Estimate regimes of validity for the model respective to the derivation assumptions.
- Compare dynamics between the coupled model and an uncoupled implementation using a linear potential field approximation. Identify effects on dynamics including the director pitch and the Fréedericksz transition.

4.2 Methodology

The previously described continuum model derived from Landau-de Gennes theory was implemented using the parameters recorded in table 4.2. These parameters correspond to

the approximate properties of 5CB at temperature of $T = 303.35°K$, $4°K$ below the supercooling temperature. Measurements of the saddle-splay constant are indirect, and have proven difficult and produced strongly varying results [55, 34, 56, 57]. Here we set $k_{24} = \frac{k_{22}}{4}$ to ensure it lies within the Ericksen limits; as this simulation uses strong anchoring, the saddle splay constant ultimately has no effect as previously discussed. Landau-de Gennes elastic constants L_i are derived from the Frank-Oseen elastic constants K_{ii} according to equations 3.23. A Dirichlet condition is used for the surface interaction, corresponding to an arbitrarily high Rapini-Papoular anchoring constant ($\alpha \to \infty$), as an implementation of strong anchoring. This anchoring penalty is necessary to isolate a single elastic mode of deformation at the exact point of transition, and offers a convenient opportunity to compare with experiment [1, 58]. This is consistent with experimental studies measuring the splay Frank-Oseen elastic constant [7], where sufficiently strong anchoring is possible and verified using the VanSprang-Yokoyama method [23].

Simulations of a nematic thin film sandwiched between uniform planar electrodes under increasing applied external field strength were conducted. The thickness of the film, $d = 5\mu m$, is consistent with experimental measurements and common LCD applications [29, 7].

The finite element mesh depicted in Figure 4.1 used to discretize the simulation domain is regular but non-uniform; element density is increased near the electrodes in order to improve convergence of the solution. Because the dynamics of the splay cell are two-dimensional, the simulation can be performed on a 2-D mesh. In order to ensure the validity of the continuum assumption, element size is kept larger than the characteristic length scales of the system. In the nematic phase, the most pertinent is the nematic coherence length, which corresponds to the thickness of a nematic-isotropic phase interface. An approximate form of the coherence length is obtained by comparing the free energy associated with the thermodynamic and elastic contributions [3]. Simplifying to the single-elastic approximation, we have:

$$\lambda_{nem} = \sqrt{\frac{L_1}{a_0 \Delta T}} \approx 3nm \tag{4.1}$$

which is easily maintained at the aforementioned domain size.

The substrate between the LC film and the electrodes creates a preferred uniformly planar orientation. This substrate is treated as infinitesimally thin. The initial alignment tensor and the preferred alignment tensor at the substrate boundry are, respectively:

$$Q_{init} = S_{eq}\left(\widetilde{\mathbf{y}} \otimes \widetilde{\mathbf{y}} - \frac{1}{3}\mathbf{I}\right), \;\; Q_{bound} = S_{eq}\left(\hat{\mathbf{y}} \otimes \hat{\mathbf{y}} - \frac{1}{3}\mathbf{I}\right) \tag{4.2}$$

where $\widetilde{y}$ is a unit vector slightly perturbed ($\theta << 1°$) from the $\hat{y}$ direction in the field-aligned direction, and S_{eq} is given by equation 3.28. This choice of initial condition corresponds

Parameter	Value	Units	Source	Parameter	Value	Units	Source
T^*_{ni}	307.35	K	[17]	K_{24}	7.75×10^{-13}	J m^{-1}	See text
a	1.3×10^{5}	J m^{-3} K^{-1}	[17]	L_1	4.28×10^{-12}	J m^{-1}	derived
b	1.6×10^{6}	J m^{-3}	[17]	L_2	1.99×10^{-12}	J m^{-1}	derived
c	3.9×10^{6}	J m^{-3}	[17]	L_3	2.68×10^{-12}	J m^{-1}	derived
K_{11}	4.45×10^{-12}	J m^{-1}	[7]	L_{24}	1.99×10^{-12}	J m^{-1}	derived
K_{22}	2.90×10^{-12}	J m^{-1}	[6]	$\epsilon_{\parallel}$	18.4	-	[7]
K_{33}	5.75×10^{-12}	J m^{-1}	[7]	$\epsilon_{\perp}$	7.2	-	[7]

to the equilibrium state of the system below the Fréedericksz transition voltage. The small perturbation of initial orientation is made to eliminate disclinations which would arise as a result of the symmetry of the cell; as the induced director of the applied field and surface anchoring are perpendicular, two opposite-handed splay textures are equally valid minimizations of the free energy [45]. In reality this symmetry is broken by locally independent thermal fluctuations in the director. The non-substrate boundaries are treated as periodic to simulate the lack of surface interaction on these axes.

The uncoupled model simulations are identical with the exception that Gauss's law is not solved and instead a linear electric field is imposed.

4.3 Results

Figure 4.2 depicts the equilibrium textures of the splay mode cell under increasing applied voltages. There exists a finite range of applied voltages under which no change in the nematic texture is induced; this is consistent with the free energy minimization theory of the Fréedericksz transition [45].

After reaching a critical Fréedericksz voltage the equilibrium texture continuously deforms in the direction of the applied voltage gradient. The texture begins to form a uniform splay-deformation structure, of handedness determined by the initial director perturbation. Two regimes of post-transition texture can be identified: in the first, the LC molecules furthest from the surface approach full alignment with the applied field, creating a sub-$\frac{\pi}{2}$ pitch

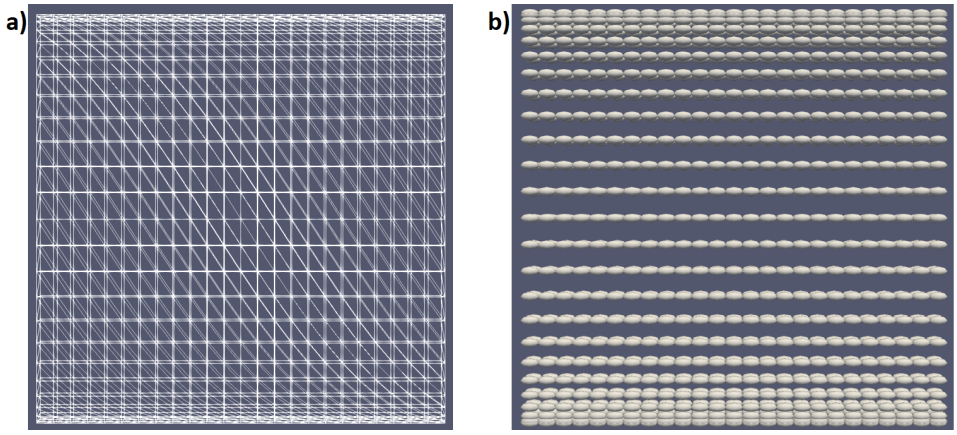

Figure 4.1: Splay mode cell mesh a) wireframe and b) glyph representations. Element size is increased continuously near the true boundaries and constant across the periodic boundaries.

structure. After the centre of the cell reaches full field alignment, the texture maintains a $\frac{\pi}{2}$ structure whose pitch decreases with increased potential.

Figure 4.3 shows the voltage dependence of the average field-aligned director component. The Fréedericksz voltage can be identified clearly from this data as $V_c = .80V$ in contrast to the experimentally recorded value [7]:

$$V_c^e = \pi\sqrt{\frac{K_{11}}{\Delta\epsilon\ \epsilon_0}} = .67V \tag{4.3}$$

This is in good agreement with work by Kilian and Hess, who also simulated a Fréedericksz transition, also reporting a simulated Fréedericksz transition voltage $V_c^{sim} \approx 1.2V_c^{exp}$ in the static regime [45]. In that work, a tensorial generalization of the Frank-Oseen model was used; this addresses the director symmetry issue but still assumes uniaxial ordering of uniform degree. As will be shown explicitly by this work's model, at the Fréedericksz transition the texture *is* uniaxial and uniformly ordered. Additionally, because the texture at the transition is uniform, field-orientation coupling should have no effect. Because of this we expect, and observe, no difference between the models in observing this specific phenomena, as shown in Figure 4.3 b).

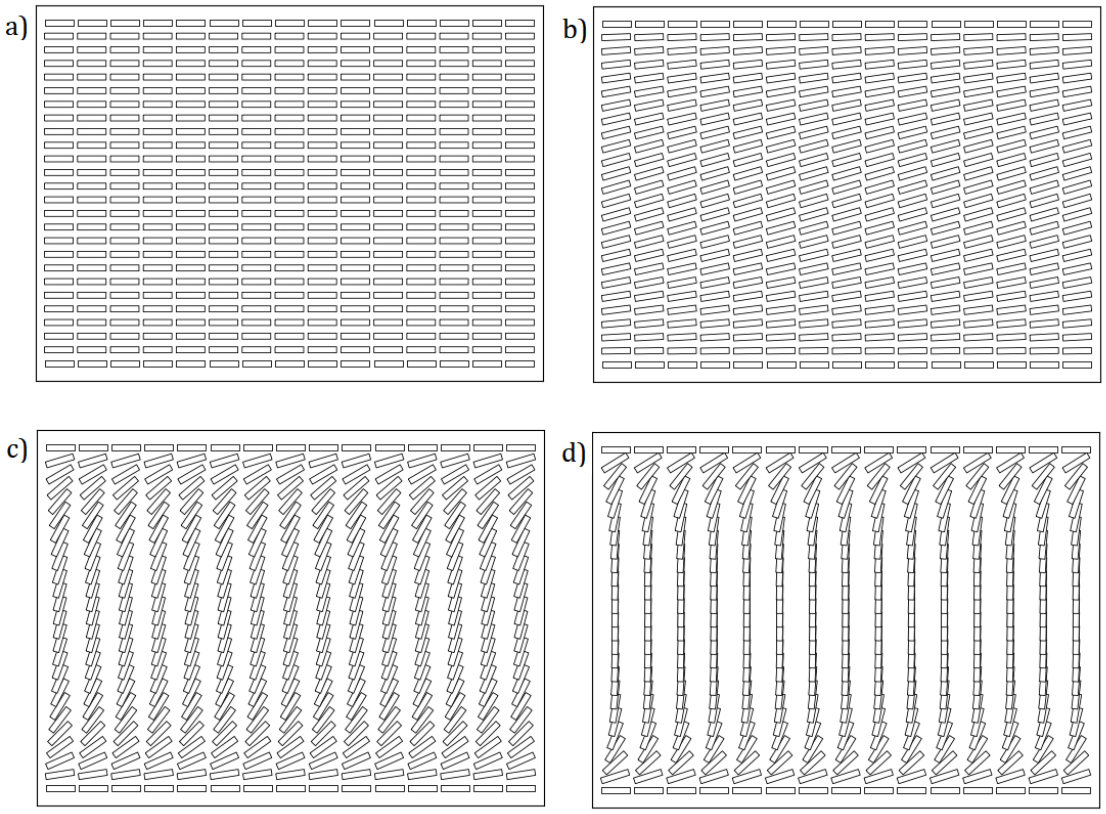

Figure 4.2: Equilibrium splay cell nematic textures for increasing voltages: 1) 0.7V b) 0.85V c) 1.4V d) 2V.

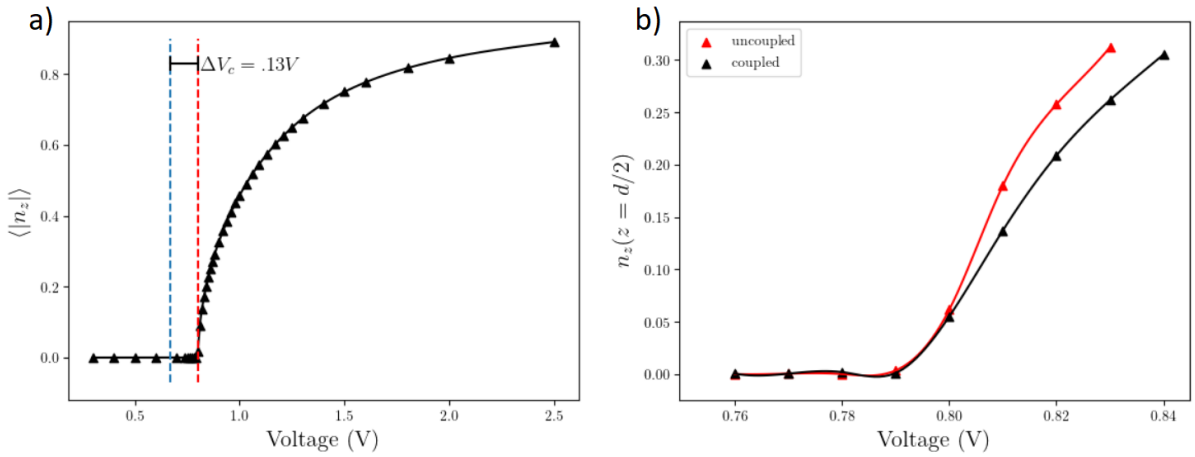

Figure 4.3: a) Average splay cell director z-component against applied voltage. Blue line indicates the transition point consistent with the reported K_{11} constant. b) Centre-cell director z-component behaviour for coupled and uncoupled model simulations at the transition voltage.

4.3.1 Validation of Approximations

Given the difference between experimental and simulated values of the the Fréedericksz transition voltage, we seek to understand this discrepancy through an investigation of the underlying assumptions of the model and the precision of its parameters.

Presence of biaxiality

Figure 4.4 shows the spatial variation of uniaxial and biaxial order parameters S and P in the Fréedericksz cell below, immediately after, and well above the critical voltage V_c. Below the transition the texture is homogenous and S is constant while the system exhibits no biaxiality. As the texture begins to reorient at $V = V_c$ biaxiality is induced commensurate to the pitch of the texture: as the voltage is further increased the pitch shortens, concentrating the biaxial ordering. The induction of biaxial order necessarily decreases uniaxial order proportionately. Because variation in S is proportional to the variation of the director in this system, it is zero at the transition point.

Figure 4.5 shows the change in electric, elastic, and bulk free energy contributions for the full system relative to the zero-field state. The transition point can easy be see again

in this plot as the point when the elastic free energy contribution becomes non-zero. The electric free energy follows the expected quadratic form. While there does exist a finite change in the bulk free energy after the transition commensurate with the variation in the uniaxial ordering, it is negligible compared to the other contributions.

The assumption of low-biaxiality used in the determination of the Landau-de Gennes elastic parameters is thus strictly valid at the Fréedericksz transition point, and should have no impact on the critical voltage. However, biaxial ordering becomes significantly present at higher voltages.

Uncertainty in model parameters

Given the validity of the model assumptions in the near-transition regime, we seek to understand the impact the precision of model parameters has on the simulated Fréedericksz voltage.

As the Fréedericksz voltage corresponds to competition between the electric and elastic free energy penalties we begin by examining the Frank-Oseen constants and dielectric anisotropy. Both of these parameters are reported to comparatively high degrees of precision [7]. Additionally, because both of these parameters are related to the transition point quadratically

$$V_c \propto \sqrt{\frac{K_{11}}{\Delta\epsilon}} \tag{4.4}$$

significant variation in the parameter space is necessary to decrease the dynamical gap. Simulations varying the elastic and electric constants within their reported ranges as expected had an unsubstantial effect of the Fréedericksz voltage.

Examining the effect of the bulk constants, which for 5CB are known to a lower precision [17], simulations were performed for a range of constant values within the reported ranges. Table 4.2 records the observed Fréedericksz voltage under several bulk parameter sets. Unintuitively, relative variance between the bulk constants has a pronounced effect on the transition, with the transition voltage ranging from .74V to .83V. Uniform variance in the parameters produced no effect on the transition voltage.

4.3.2 Impact of Field-Orientation Coupling

Following the validation of the model against experimental data, we seek to quantify the impact that coupling between the molecular order and applied field have on the model dynamics. It is common to impose uniform or ad-hoc fields [12, 44, 48], however the explicit

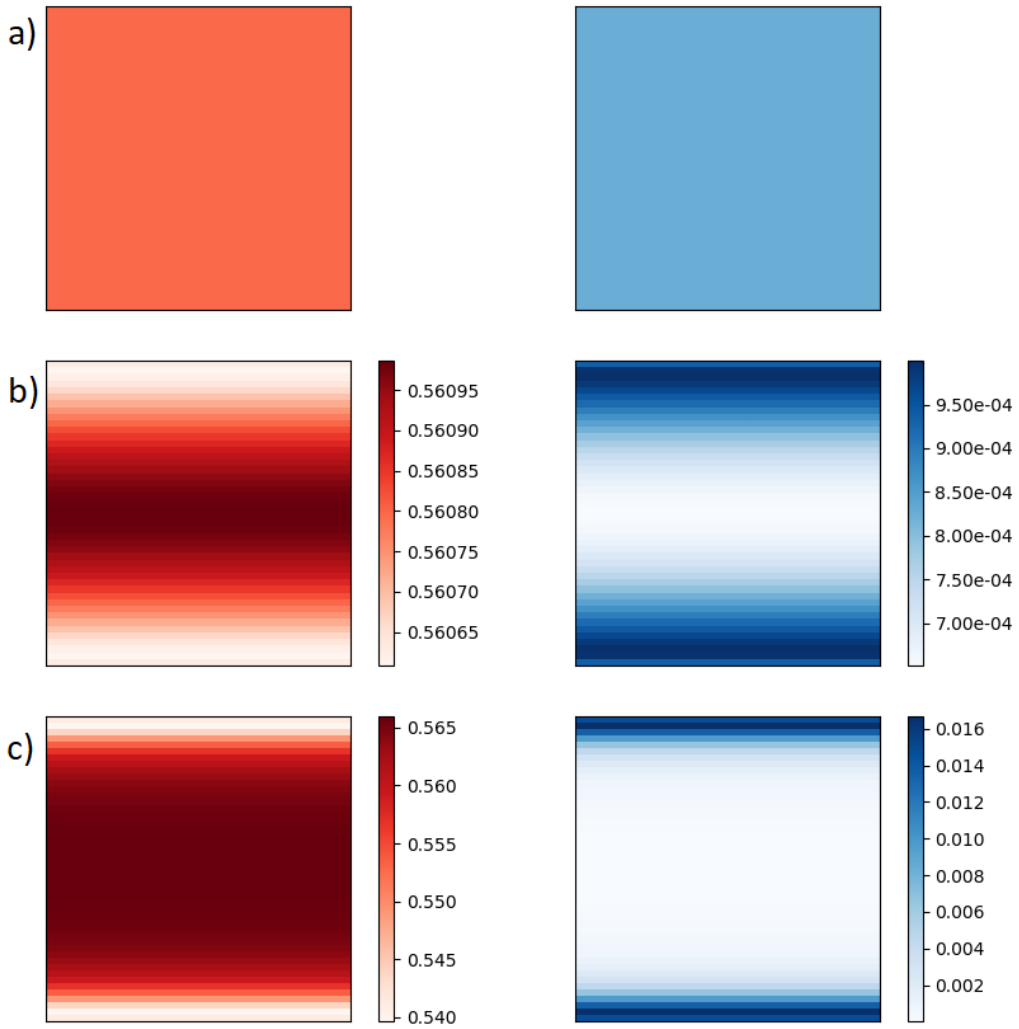

Figure 4.4: Spatial variation in uniaxial order parameter S (Reds) and biaxial order parameter P (Blues) in the $\Delta T = 4°C$ splay modulus cell at a) 0.7V b) 0.82V c) 2V

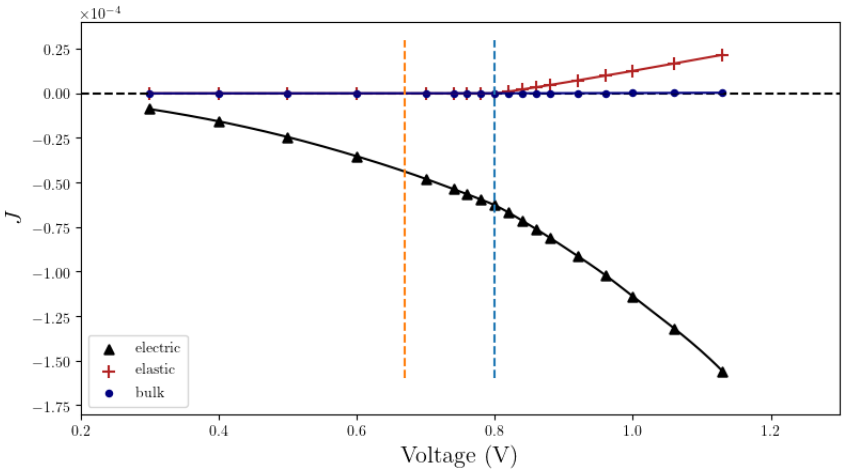

Figure 4.5: Changes in free energy against applied voltage. The blue and orange lines denoted the simulated and experimental Fréedericksz voltages, respectively. Note that the variation in the bulk free energy is negligible in comparison to the elastic and electric contributions.

$a\ [Jm^{-3}K^{-1}]$	$b\ [Jm^{-3}]$	$c\ [Jm^{-3}]$	V_c	$V_c - V_c^e$
1.4×10^5	1.8×10^6	3.6×10^6	.83	.16
1.4×10^5	1.6×10^6	3.9×10^6	.81	.14
1.3×10^5	1.6×10^6	3.9×10^6	.8	.13
1.3×10^5	1.4×10^6	4.2×10^6	.74	.07
1.3×10^4	1.4×10^5	4.2×10^5	.74	.07
1.3×10^3	1.4×10^4	4.2×10^4	.74	.07

Table 4.2: Fréedericksz voltages exhibited by the model associated with different bulk parameter sets and the variation from experimental value. The first four sets correspond to values within the experimentally reported ranges; the final two sets are arbitrarily and uniformly reduced.

accuracy of these approximations is often not well quantified. Additionally, while many extensive properties of the system may be largely invariant under uncoupled approximations, it is instructive to see what dynamics are potentially being obscured. Here we examine the effect of accounting for coupled interactions on the Fréedericksz transition, the electric field, and the nematic texture.

Simulations identical to those described immediately above were performed with the uncoupled solver; Gauss's Law was not solved simultaneous to the free energy minimization which instead assumed a linearly increasing electric potential and thus constant electric field across the cell.

Figure 4.3 b) shows the voltage dependence of the field-aligned director component of the cell centre under coupled and uncoupled simulation. The Fréedericksz transition occurs at the same applied voltage as the coupled model, as it must since uniformity in the alignment tensor at the transition corresponds to a linearly increasing electric field.

Figure 4.6 a) shows the coupled equilibrium potential function across the splay-mode cell in comparison to the linear approximation at $V = 4.0$. Figure 4.6 b) shows the difference in potential profiles (uncoupled - coupled) across the cell at several voltages. At applied voltages near the Fréedericksz transition a sinusoidal deviation from the linear form follows the extended deformation of the phase. At higher voltages, where the centre of the cell is strongly-field aligned, the deviation is confined to an increasingly smaller section near the surface, congruent to the high pitch of the rotating director.

Figure 4.7 shows the electric field at equilibrium for a) V = 0.85 and b) V = 4.0 in contrast to the constant-field approximation. As the applied voltage is increased, the variation of E from its mean value is significantly increased and again concentrated along the pitch of the rotating director. Table 4.3 records the variation in the electric field at additional voltages.

4.4 Summary

Continuum simulations were performed to validate the implemented Landau-de Gennes model against experimentally observed data and to understand the precision of the model as a function of the precision of the model parameters. The expected dynamics associated with the Fréedericksz transition was observed within close (≈20%) proximity to the value observed by Bogi and Faetti in their comprehensive study of the material [7]. The discrepancy initially suggests a significant correction to the elastic or electric parameters, however closer investigation of the bulk constants showed that the transition dynamics

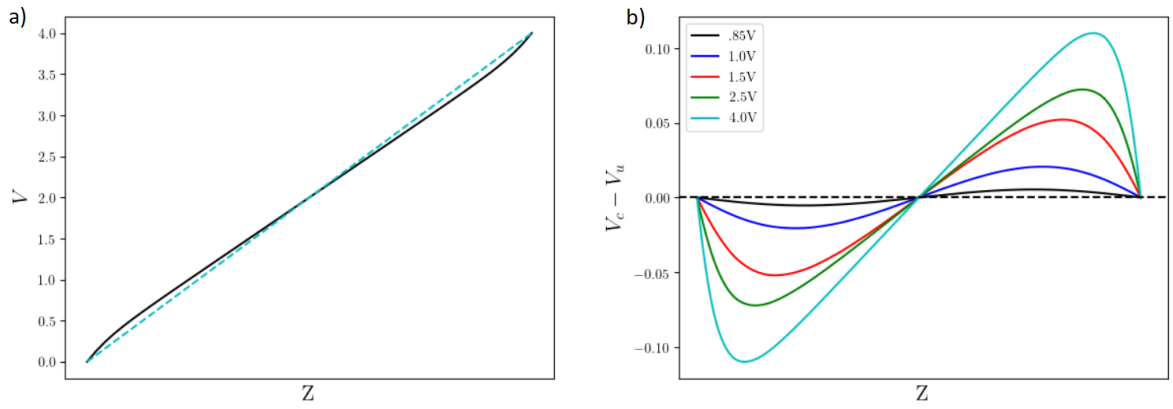

Figure 4.6: Comparisons of the potential field between simulation and linear approximation. a) Simulation potential [black] and linear potential [blue] across cell thickness at 4V. b) Difference (uncoupled-coupled) in potential fields across cell thickness for several applied voltages.

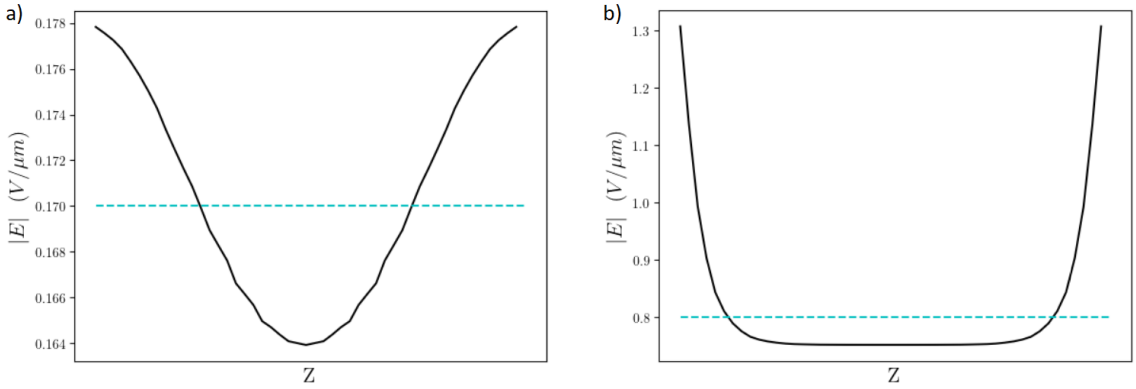

Figure 4.7: Comparisons of the electric field profiles between simulation [black] and linear [blue] approximation for the splay-mode cell at a) $V = 0.85V$ b) $V = 4V$.

V	E_{max}	E_{min}	E_{lin}
.85	.178	.164	.170
1.0	.237	.182	.200
1.5	.412	.261	.300
2.0	.597	.360	.400
4.0	1.31	.751	.800

Table 4.3: Maximum and minimum electric field ($V/\mu m$) at simulation equilibrium versus a linear aproximation for several applied voltages.

were strongly affected by the relative value of the thermodynamic parameters. This is not immediately obvious as the change in bulk free energy is proportional to the spatial variation of the alignment tensor, which is (and was verified to be) near-constant at the transition point. Additionally, it is only the relative variance of the thermodynamic constants which impacts the cell dynamics - an arbitrary factor applied to all bulk parameters created no change in Fréedericksz voltage or nematic texture. This leads to the unobvious conclusion that the less-precisely known thermodynamic constants can have a significant impact on the simulated dynamics of the Fréedericksz cell.

Additionally, a parameter combination belonging to the reported space was not found which matched experiment with high precision. This suggests that beyond concerns with parameter values, the truncation of the Landau expansion chosen in the model could be re-examined. There exists literature wherein models are expanded to fifth order in the alignment tensor, or third order in the alignment tensor gradients, however this necessarily introduces an increasing bevy of additional thermodynamic and elastic parameters which are themselves difficult to measure with precision.

The splay-mode cell was found to exhibit low, if non-trivial biaxial ordering under voltage ranges commonly associated with industrial use of liquid crystalline thin films. $P = .02$ was observed at 3.0V, with S varying by a congruent amount. This is relevant to model precision as the Landau-de Gennes elastic constants are derived from the much more easily observed Frank-Oseen elastic constants under the assumptions of the Frank-Oseen formalism (wherein uniaxial ordering is assumed constant, and biaxial ordering is assumed non-existent).

Evaluating the assumptions of the model explained our good agreement with Kilian and Hess, whose model approximations should become completely negligible at the Freed-

ericksz transition point. That we agree with experiment reasonably well and to previous work extremely well supports the validation of the model. We show explicitly that the discrepancy with experiment is not due to biaxial ordering or non-uniform uniaxial ordering. This suggests that the discrepancy is due to an additional free energy not included in the models, such as thermal fluctuations or the flexoelectric free energy contribution recently presented by Kim et al [29]. Alternatively, because the elastic parameters are ultimately calculated using Frank-Oseen theory, the discrepancy between model and experiment could be understood as arising from the limited order of the Frank-Oseen model. Lastly, uncertainty in the relative values of the bulk constants could again be partially responsible. The impact of using a higher order in the Landau-de Gennes bulk constants could similarly be non-negligible because of this.

Ultimately the implemented model can be understood to model field-induced nematic textures to a practical degree of precision. The dynamics associated with the coupled relationship between molecular orientation and external fields was studied, with significant spatial variation in the electric field found at voltages above the Fréedericksz transition. This non-uniformity demonstrates the importance of solving Gauss's Law simultaneous to the free energy minimization in systems where the molecular director varies strongly over the domain at equilibrium.

Chapter 5

Simulation of IPS Cells

5.1 Overview

Continuing on the previous preliminary study, we now model the dynamics of more complex and industrially relevant systems. This work simulates in-plane-switching (IPS) liquid crystal display cells consistent with modern applications. At the crux of IPS development is the careful optimization of intimately related and frequently conflicting cell properties; ideal balances of anchoring strength against electric field strength, field eccentricity against applied voltage, and switching-time against all of the above necessitate accurate predictive simulations of cell dynamics.

We first study the effect of the structure of the applied electric field on the equilibrium state of such cells, characterizing the competition between the surface and electric free energies which drives the dynamics of the system. This is manifest in the electrode configuration and voltage differential applied.

With an understanding and demonstration of the nematic phase's behaviour across different regimes of the parameter space, we then have the proper context with which to study the impact of coupling between molecular ordering and external electric fields on the dynamics of IPS cells. We compare qualitatively and quantitatively the dynamics predicted by our model against those predicted using stringent contemporary approximations.

The specific goals of this work are:

- Study the effects of electrode placement and applied voltage strength on the equilibrium ON-state texture of IPS cells. This is primarily within the context of consider-

ing the effect on cell transmittance, examining director and electric field uniformity throughout the domain.

- Study the performance of the coupled model relative to contemporary approximations of the potential field for IPS systems. Additionally, characterize the types of dynamics lost under such ad-hoc solutions.

- Demonstrate the ability of the model to accurately compute arbitrary electrode and domain configurations associated with modern LCD application.

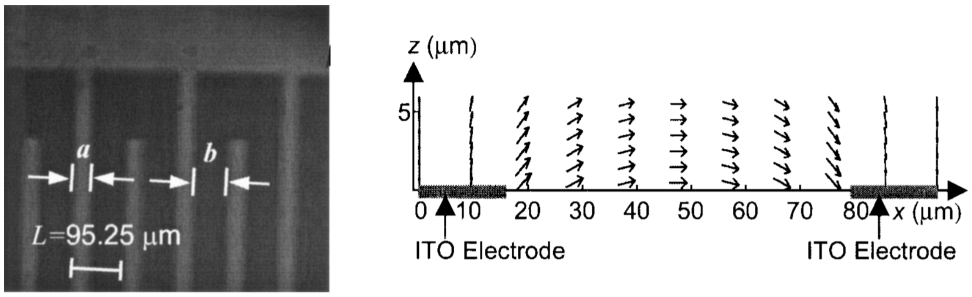

Figure 5.1: SEM image of interdigital electrodes associated with IPS construction. Electric field configuration in an IPS cell. From ref [14].

5.2 Methodology

The model parameters used are identical to the previous section, shown in table 4.2, with the additional inclusion of a finite anchoring energy constant, $\alpha = 5\times10^{-4} J/m^2$. This value is consistent with rubbed-polymer surfaces, which exhibit anchoring energies on the order of $10^{-4} - 10^{-5} J/m^2$ [59]. The anchoring energy is then implemented as a Rapini-Papoular contribution of the form:

$$f_{surf} = \frac{1}{2}\alpha(Q - Q^s)^2 \tag{5.1}$$

where the preferred order parameter at the surfaces is given by:

$$Q^s_{z=d} = S_{eq}\left(\hat{x} \otimes \hat{x} - \frac{1}{3}\delta\right) \tag{5.2}$$

$$Q^s_{z=0} = S_{eq}\left(\hat{y} \otimes \hat{y} - \frac{1}{3}\delta\right) \tag{5.3}$$

with $\hat{z}$ being across the cell thickness and with the equilibrium uniaxial order parameter given by equation 3.28 as:

$$S_{eq} = \frac{b}{4c}\Big(1 + \sqrt{1 - 24(a_0(T - T^*_{ni})c/b^2)}\Big) = .6070 \tag{5.4}$$

The IPS domain consists of a thin liquid crystalline film patterned on one side with interdigital electrodes of uniform width w and separation s, a configuration depicted in Figure 5.1. Each set of interlocked 'fingers' is connected away from the domain, creating alternating strips of positive and negative potential. For a film of thickness d, $\frac{d}{s} > 1$ corresponds to a predominately horizontal electric field in the plane of the film across the patterned electrodes. To allow for proper periodicity, two IPS cells are simulated on a domain containing a half-thickness positive electrode, a negative electrode, and a second half-thickness positive electrode.

An identical meshing practice to the previous chapter is used, creating a regular but non-uniform mesh which increases in density near the electrodes. Alternating electrodes are treated as being connected far away from the system, such that they may be treated as infinitely long strips. Electrodes are considered Dirichlet potential bounds alternating across the $\hat{x}$ axis, and the non-substrate boundaries are again treated as periodic.

The simulation initial condition (Figure 5.2)is consistent with the equilibrium position of an OFF-state IPS cell:

$$Q_{init} = S_{eq}\Big(n_{init}n_{init} - \frac{1}{3}\delta\Big) \tag{5.5}$$

The initial director represents a 90° twist in the plane of the film:

$$\hat{n_{init}} = \sin(\frac{\pi}{2}\frac{z}{d})\hat{x} + \cos(\frac{\pi}{2}\frac{z}{d})\hat{y} \tag{5.6}$$

The initial condition for the potential field is a uniform gradient across the electrodes:

$$V_{init} = \frac{\Delta V x}{2w + s} \tag{5.7}$$

This is chosen simply as a convenient initial guess for the ideal behaviour of the potential field, which is then iterated towards the true value. Remaining conscious of the inherent length scales involved with the continuum model, we compare the competition between different free energies to obtain characteristic distances. We will again revert to the single-constant elastic approximation as we are only interested in the approximate orders of magnitude. Comparing electric and elastic free energies we have

$$\lambda_e = \sqrt{\frac{L_1}{\Delta\epsilon\epsilon_0 E^2}} \tag{5.8}$$

a dielectric coherence length. For the parameters listed, this length scale is at most approximately 80nm.

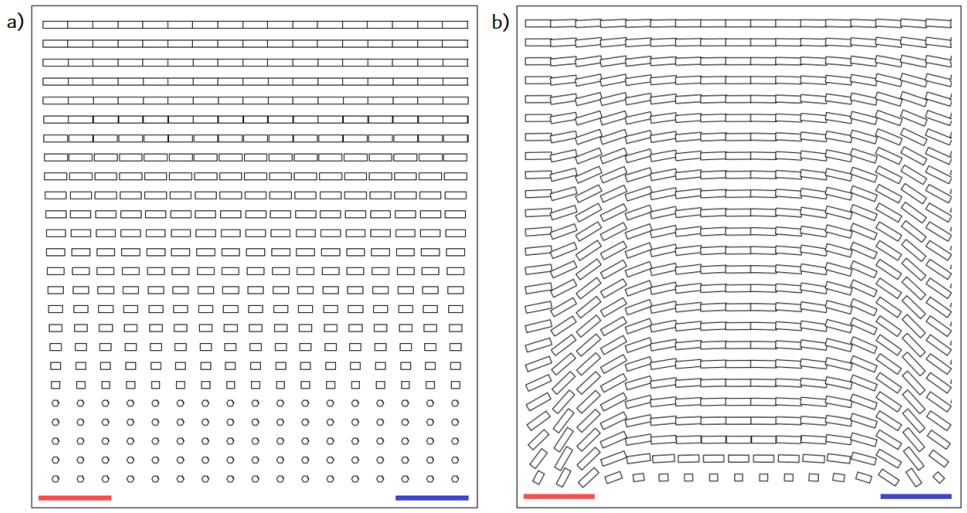

Figure 5.2: OFF- and ON-state director textures for an IPS cell with dimensions $s = 10\mu m$, $w = d = 5\mu m$, and voltage differential $V = 24V$ across the positive [red] and negative [blue] electrodes. Image dimensions are resized and only a fraction of mesh elements are vizualized for clarity.

5.3 Results

5.3.1 Investigation of Electrode Patterning

Simulations of in-plane switching cells with the domain parameters $w = 5\mu m$, $d = 5\mu m$, $V = 24V$ were performed under a set of electrode spacing distances ranging $5\mu m \leq s \leq 25\mu m$. A voltage differential of $24V$ was chosen because it represents a reasonable value in the practical engineering of IPS devices and allows for a wide range of electrode separation distances to be considered. Figure 5.3 shows equilibrium director fields of the ON-state for increasing values of s.

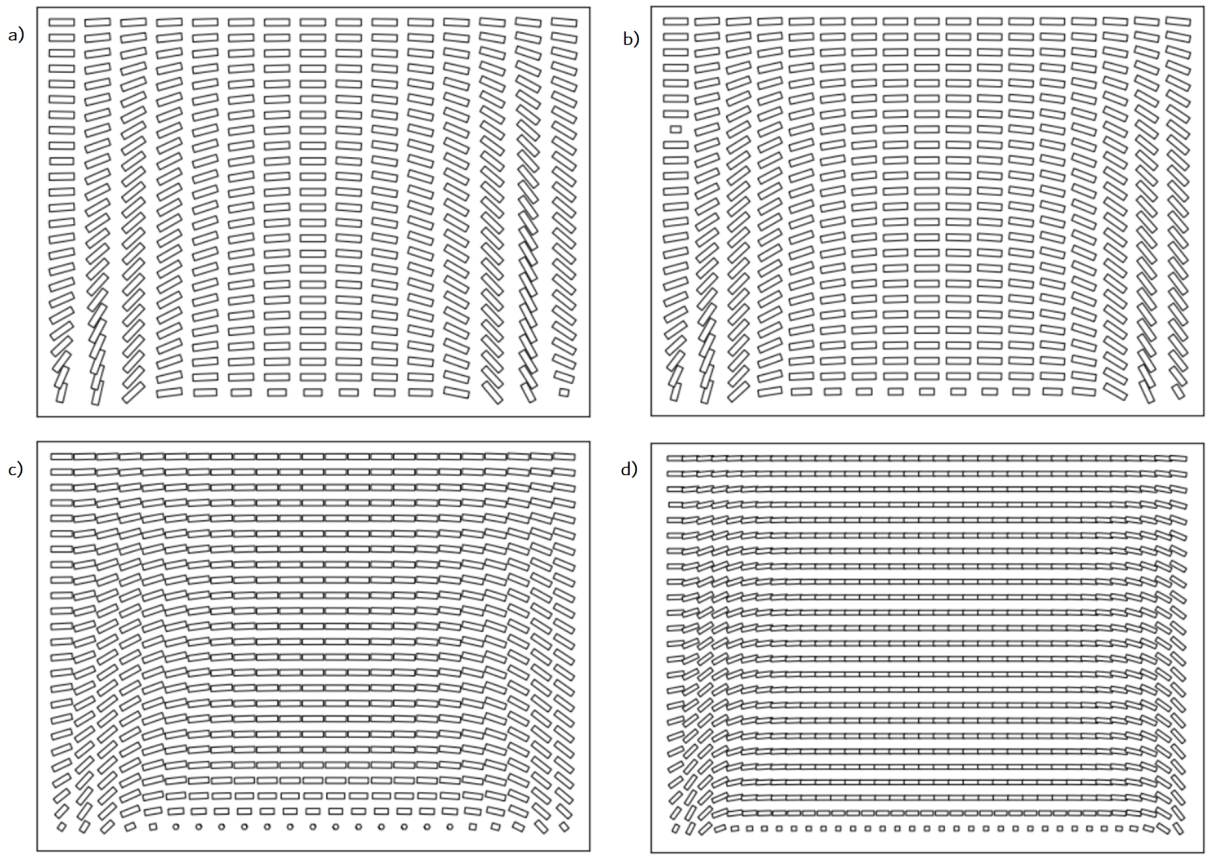

Figure 5.3: ON-state director textures for an IPS cell with voltage differential $V = 24V$ and dimensions, $w = d = 5\mu m$ and a) $s = 7.5\mu m$ b) $s = 10\mu m$ c) $s = 15\mu m$ d) $s = 25\mu m$.

The immediately obvious benefit to increasing separation distance is readily apparent in Figure 5.3, where the decreasing $\frac{d}{s}$ ratio results in a more consistently horizontal director texture between the interdigital electrodes. This corresponds to the electric field itself becoming less eccentric as well as the increased lengthscale over which the texture may elastically deform.

At a separation distance between $5\mu m \leq s \leq 7.5\mu m$, the twist structure of the OFF-state initial condition ceases to be unwound, with the pitch at ON-state equilibrium increasing with further separation. This is an immediate consequence of the electric field decreasing in strength as the potentials are moved apart, and the surface interaction thus failing to be sufficiently overwhelmed.

Figure 5.4 a) shows the $\hat{y}$ (anchoring-aligned) component of the director across the cell thickness at the central point (the *optical pathway*) between the electrodes at various separations of the ON-state. At $s < 7.5\mu m$, the director field is completely unwound at the surface. As s is increased past $7.5\mu m$, the director becomes anchoring-aligned at the lower surface and exhibits a twist of increasing pitch.

Figure 5.4 b) shows the $\hat{x}$ (field-aligned) component of the director along the cell width at $z = \frac{d}{2}$. The breadth of strongly $\hat{x}$-aligned nematic increases with separation as the field eccentricity lowers. This is ideal for creating a wide region through which to transmit light through the cell. It can be argued from this data that there exists no appropriate separation distance within this parameter set which both sufficiently unwinds the initial condition and produces a reliable horizontal texture of significant width; thus it may be concluded that either the surface interaction strength α should be lowered or the voltage increased. One should remain cognizant that the former will increase cell switching time between the states. In practice a wide range of cell separations, anchoring interactions, and voltages are found in IPS systems.

5.3.2 Impact of Field-Orientation Coupling

The previous simulations of IPS cells with varied electrode separation distances were reperformed using a model which did not couple the electric potential field to the molecular orientation. In this model, the potential field is held constant throughout all timesteps at the values corresponding to an isotropic 5CB medium. Figure 5.5 depicts this potential. This represents arguably the most stringent approximation against which to compare the coupled model, as the only way to improve upon this approximation would require knowledge of molecular orientation. This uncoupled model is a direct modification of the

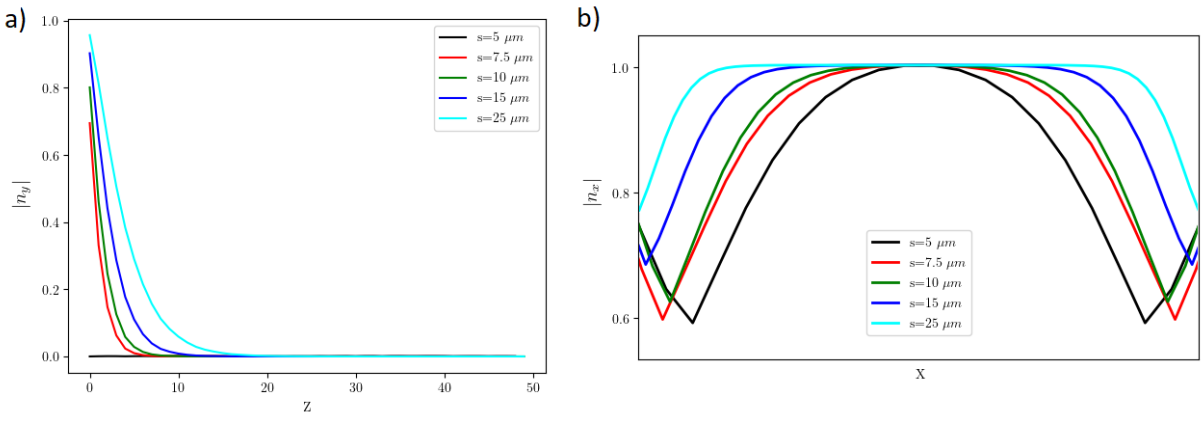

Figure 5.4: a) Director y-component across IPS cell thickness at midway between electrodes. b) Director x-component along electrode plane midway through cell thickness.

previously described model. All other initial conditions and model parameters are identical to the coupled model.

Figure 5.6 shows the difference in the equilibrium director field for an IPS cell whose ON-state exists at the cusp of unwinding the OFF-state twist texture. This parameter set is chosen as a characteristic example because the unwinding transition is of primary relevance to the cell's transmittance. The alignment behaviour in the bulk is qualitatively similar for both models, though the uncoupled simulation exhibits a generally weaker anchoring-aligned texture at the lower substrate. The difference in director alignment is strongly localized to the areas directly above the electrodes, with the comparatively homogenous textures of the optical pathways being similar to within 1% away from the lower substrate.

These effects can be seen more clearly in Figure 5.7, which depicts the difference in field-aligned director components between the models; the behaviour at the lower substrate is noticeably different between the models near the unwinding transition. However, repetition of the above separation distance study showed the unwinding transition is not significantly affected by the coupling approximation.

5.3.3 Presence of Biaxiality

We are interested in examining the presence of biaxial ordering in these systems, both to the illustrate the necessity of using the biaxial Landau-de Gennes model and to con-

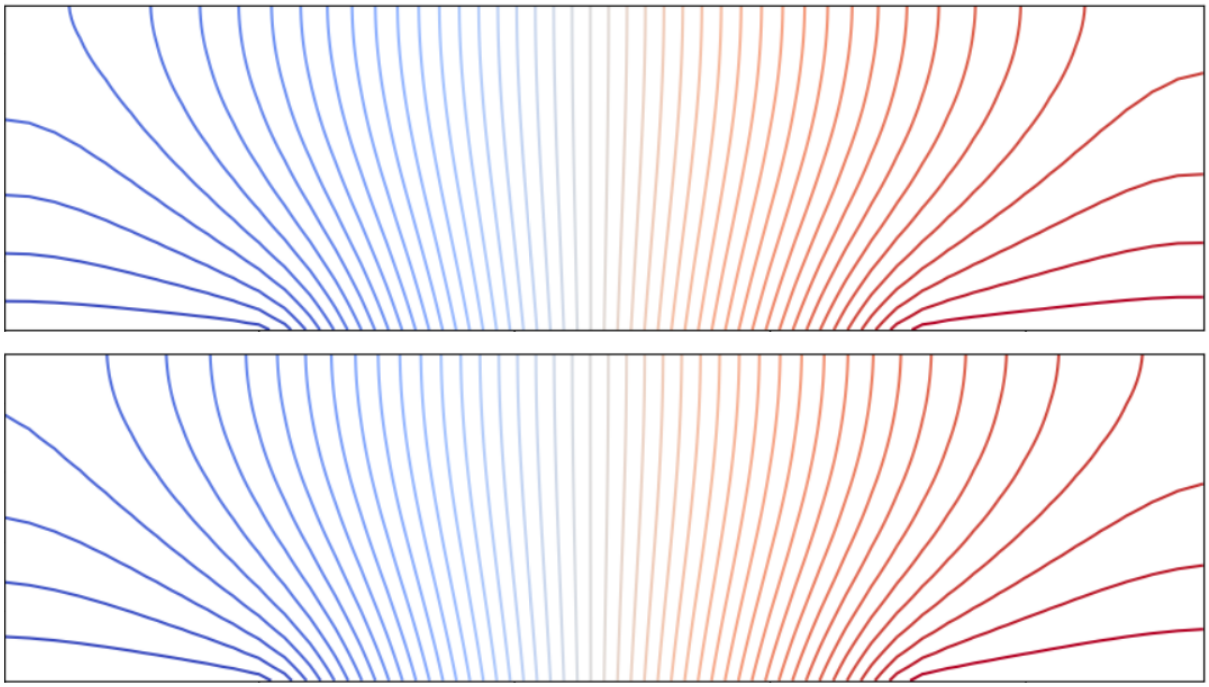

Figure 5.5: Lines of equipotential for the IPS ON-state at equilibrium using the [top] coupled model [bottom] uncoupled model with the isotropic dielectric constant approximation.

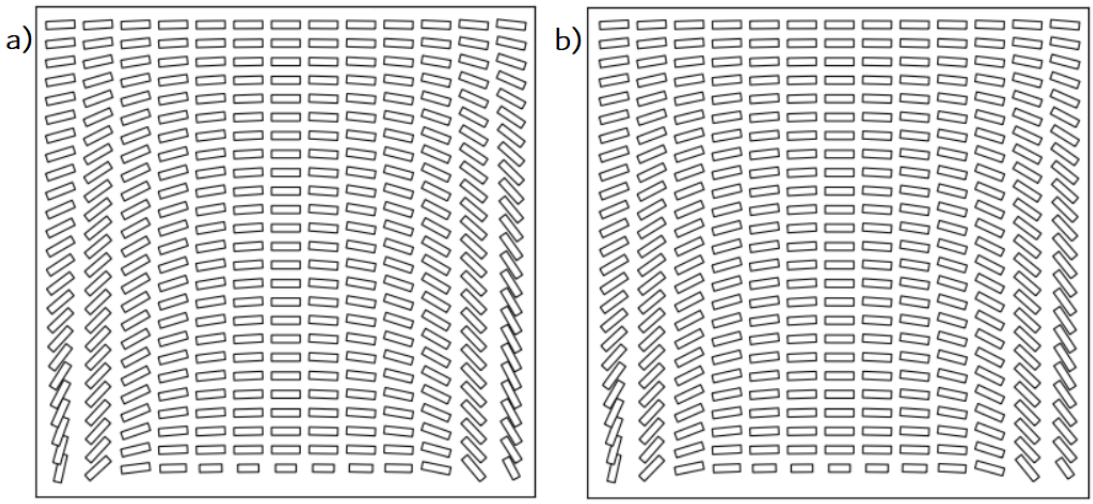

Figure 5.6: Equilibrium ON-state textures for uncoupled [left] and coupled [right] simulations of IPS cells with parameters $w = 5\mu m$ $d = 5\mu m$ $s = 10\mu m$ $V = 24V$.

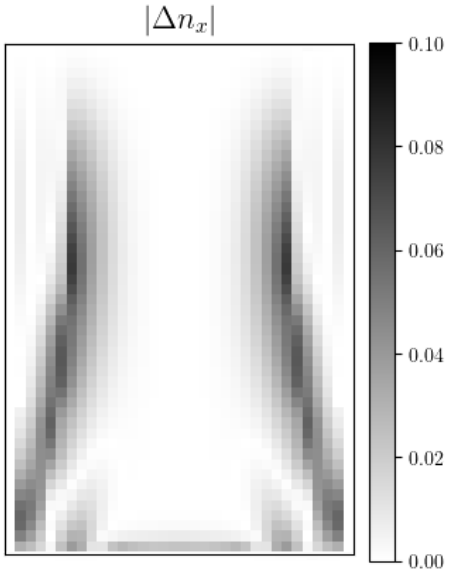

Figure 5.7: Absolute difference in director $\hat{x}$ component between coupled and uncoupled simulations with parameters $w = 5\mu m$ $d = 5\mu m$ $s = 7.5\mu m$ $V = 24V$.

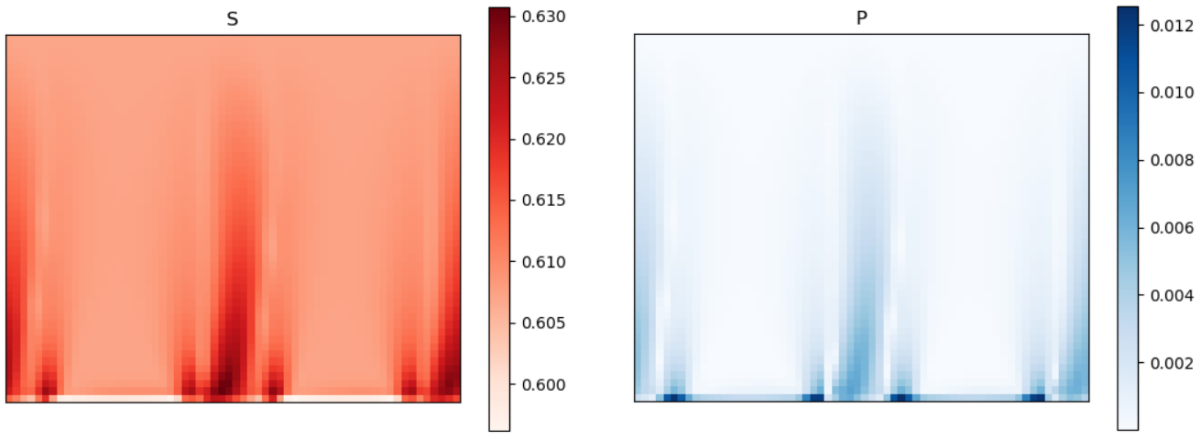

Figure 5.8: Degrees of [left] uniaxial and [right] biaxial ordering within an IPS cell with parameters $w = 5\mu m$ $d = 5\mu m$ $s = 7.5\mu m$ $V = 24V$.

sider the impact on the elastic parameters derived from Frank-Oseen theory. Unlike the earlier Fréedericksz cell system, biaxial ordering is expected to be non-trivial under the competition between the surface, elastic and electric free energies which drives the IPS cell transition.

Figure 5.8 shows the presence of uniaxial and biaxial ordering in the IPS ON-state for a parameter set near the point where electric field strength ceases to overwhelm the surface effect at the lower substrate. Near this unwinding point, strong competition between the perpendicular anchoring and electric effects induce biaxiality near the lower substrate, with $P = .012$ quickly decaying to near non-existence within the bulk of the optical pathway. A commensurate 6% variation in S near the substrate necessarily coincides with the induced biaxial ordering. It can be seen that the electric field increases the ordering of the phase away from the surface. The presence of biaxiality limits the accuracy of the elastic parameters of the model as represented in that region, however it also highlights the need for the Landau-de Gennes theory in describing even defect-free systems to a high degree of fidelity.

5.4 Summary

Continuum simulations of in-plane switching liquid crystal display cells were performed under a variety of electrode configurations and under both a coupled and uncoupled model.

We were able to study the equilibrium behaviour of the IPS ON-state as a function of applied electric field strength and eccentricity, observing three regimes of textures. At low electrode separation distances, the field eccentricity prevented in the optical pathway sufficiently uniform and purely horizontal molecular alignment, which diminishes the ON-state transmittance. At a middle regime of electrode separations the optical pathway texture was substantially horizontal. At higher separation distances, the electric field strength was insufficient to overpower the anchoring effect, and as a result the OFF-state twist was not fully unwound. This has a pronounced effect on cell transmittance as the presence of the twisting structure rotates incident light polarizations.

Comparing IPS simulations between the coupled and uncoupled model, we observed similar electric potential fields and optical pathway bulk behaviour. Nematic texture near and above the electrodes exhibited significant differences in director, however as the pertinent properties of the cell are dependent on the optical pathway, optical properties are largely unaffected by the coupling interaction. The uncoupled model underpredicts the degree of field-alignment at the substrate, even when using the most stringent possible approximation.

Ultimately, while coupling between the electric field and molecular orientation in liquid crystal systems has been accounted for in some previous works, we have examined and quantified the specific impact of this consideration on the critical dynamics of industrially relevant systems. We find that while coupling has a pronounced effect on some cell properties, the relevant characteristics of the cell are not significantly misrepresented under uncoupled approximations. This supports the many contemporary works which omit field-orientation coupling for design optimization of these systems, while also demonstrating that coupling has a pronounced impact on complex textures generally.

Additionally, we demonstrate that the generality and modularity of the model justify its candidacy as a tool for the engineering and optimization of LCD systems. The ability to specify arbitrary configurations of electrodes and surface interactions while requiring no foreknowledge of the equilibrium electric field makes the presented work useful for simulating a wide range of highly specific LCD devices.

Chapter 6

Conclusions

6.1 Conclusions

In this work, there has been implemented a continuum simulation of thermotropic nematic liquid crystals using the Landau-de Gennes model with proper accounting for the inherent coupling between molecular ordering and external electric fields through the simultaneous solving of the macroscopic formulation of Gauss's law for dielectrically anisotropic media. This most general description of nematic phases was implemented without common approximations including the single elastic constant and (when appropriate) strong-anchoring approximations.

The precision of this model and its susceptibility to uncertainty in its parameters was assessed within the common experimental paradigm of the Fréedericksz transition, with the following primary conclusions:

- Model performance at the Fréedericksz transition point was consistent with earlier works. This is expected as the improvements of this model over previous works confers no benefit when the electric field at equilibrium is already precisely known, and instead serves as a validation of the model.
- The relative, not absolute, values of the bulk constants were found to have a pronounced effect on the Fréedericksz voltage predicted by simulations. This indicates that model dynamics are significantly affected by the precision of these constants even in regimes where the change in bulk free energy is negligible in comparison to the elastic and electric contributions.

- The impact of typical model approximations, notably the derivation of the Landau-de Gennes elastic constants from the Frank-Oseen elastic constants via uniform uniaxiality, was assessed. It was shown explicitly that at the transition point, these approximations become negligible. Thus we conclude the discrepancy is linked to other factors, including the limited order of the Frank-Oseen model and absence of thermal fluctuations.

Additionally a study of the model in using a more complex nematic texture, the in-plane switching LCD cell, was performed in the interest of understanding first the dynamics omitted by uncoupled models in systems with complex textures, and secondly to demonstrate the utility of the model in the design and optimization of these systems. The following primary conclusions are made:

- There exists a significant discrepancy between the predicted ON-state textures of the IPS cell between the coupled and uncoupled models. Behaviour of the nematic director at and above the patterned electrodes was substantially different. While pertinent cell optical properties are unsensitive to this difference, coupling can be seen to nontrivially impact texturally complex nematics.
- The developed model is of practical use in the optimization of these LCD cells; allowing an examination of the effects of the many tunable parameters on the state of the liquid crystal phase. The model allows the simulation of irregular and non-uniform domains, arbitrary electrode configurations, and arbitrary combinations of surface interactions.

Thus we stress the importance of not only eschewing approximations in the modelling of these systems as is generally known, but understanding explicitly the impact of these assumptions on the predictions and precision of the models.

6.2 Recommendations

The presented model represents a state-of-science description of nematic liquid crystal phases, drawing from a wide body of contemporary work to be as general as possible. However, there still exists further room for improvements; accounting for additional free energy contributions such as thermal fluctuations or the flexoelectric contribution described

recently by Kim et al. [29] could improve the accuracy of the model in describing phenomena near the nematic-isotropic phase transition and in densely varying textures, respectively. Although flow is considered negligible in the studied systems, hydrodynamical considerations could extend the model to study additional systems wherein the hydrostatic assumption is not reasonable. These improvements are non-trivial, however may be worthwhile with increasing engineering interest in high-fidelity simulation of such systems.

It would also be of great interest to numerically simulate the optical properties of the simulated textures, especially with regard to transmittance ratios and birefringence. The lack of consistent paraxial alignment in the IPS cells requires use of the [2x2] extended Jones matrix method for transmittance, whose implementation into the finite element framework would be non-trivial [29]. Since these are the properties which ultimately drive design and optimization, a more explicit understanding of their behaviour is pertinent.

References

[1] Robert H Chen. *Liquid crystal displays: fundamental physics and technology*. John Wiley & Sons, 2011.

[2] Peter J Collings and Michael Hird. *Introduction to liquid crystals: chemistry and physics*. CRC Press, 2017.

[3] Maurice Kleman and Oleg D Laverntovich. *Soft matter physics: an introduction*. Springer Science & Business Media, 2007.

[4] Frederick C Frank. I. liquid crystals. on the theory of liquid crystals. *Discussions of the Faraday Society*, 25:19–28, 1958.

[5] Pierre-Gilles De Gennes and Jacques Prost. *The physics of liquid crystals*, volume 83. Oxford university press, 1993.

[6] GR Luckhurst, David A Dunmur, and Atsuo Fukuda. *Physical properties of liquid crystals: nematics*. Number 25. IET, 2001.

[7] A. Bogi and S. Faetti. Elastic, dielectric and optical constants of 4'-pentyl-4-cyanobiphenyl. *Liquid Crystals*, 28(5):729–739, 2001.

[8] Chinnaiyan Selvarasu and Palaninathan Kannan. Bent shaped 1,3,4-oxadiazole/thiadiazole heterocyclic rings containing liquid crystals. *Journal of Chemical Sciences*, 127(10):1831–1838, Oct 2015.

[9] Sophie A Jones, James Bailey, David RE Walker, Guy P Bryan-Brown, and J Cliff Jones. Method for tuneable homeotropic anchoring at microstructures in liquid crystal devices. *Langmuir*, 34(37):10865–10873, 2018.

[10] BBCLCD. Schematic diagram ips lc display. https://commons.wikimedia.org/wiki/File:DiagramLCDIPS. Accessed: 2019-07-04.

[11] WH De Jeu, WAP Claassen, and AMJ Spruijt. The determination of the elastic constants of nematic liquid crystals. *Molecular Crystals and Liquid Crystals*, 37(1):269–280, 1976.

[12] CZ Van Doorn. Dynamic behavior of twisted nematic liquid-crystal layers in switched fields. *Journal of Applied Physics*, 46(9):3738–3745, 1975.

[13] Hiroyuki Mori, Eugene C Gartland Jr, Jack R Kelly, and Philip J Bos. Multidimensional director modeling using the q tensor representation in a liquid crystal cell and its application to the π cell with patterned electrodes. *Japanese journal of applied physics*, 38(1R):135, 1999.

[14] Haiqing Xianyu, Sadeg Faris, and Gregory P Crawford. In-plane switching of cholesteric liquid crystals for visible and near-infrared applications. *Applied optics*, 43(26):5006–5015, 2004.

[15] Fred Fu. Formation and field-switching dynamics of nematic droplets, 2017.

[16] Joseph A Castellano. *Liquid gold: the story of liquid crystal displays and the creation of an industry*. World Scientific, 2005.

[17] HJ Coles. Laser and electric field induced birefringence studies on the cyanobiphenyl homologues. *Molecular Crystals and Liquid Crystals*, 49(3):67–74, 1978.

[18] Monika Gupta and Santanu Kumar Pal. The first examples of room temperature liquid crystal dimers based on cholesterol and pentaalkynylbenzene. *Liquid Crystals*, 42(9):1250–1256, 2015.

[19] Zhang Ran, He Jun, Peng Zeng-Hui, and Xuan Li. Calculating the dielectric anisotropy of nematic liquid crystals: a reinvestigation of the maier–meier theory. *Chinese Physics B*, 18(7):2885, 2009.

[20] Muhammad Arslan Shehzad, Dung Hoang Tien, M Waqas Iqbal, Jonghwa Eom, JH Park, Chanyong Hwang, and Yongho Seo. Nematic liquid crystal on a two dimensional hexagonal lattice and its application. *Scientific reports*, 5:13331, 2015.

[21] J Stöhr and MG Samant. Liquid crystal alignment by rubbed polymer surfaces: a microscopic bond orientation model. *Journal of electron spectroscopy and related phenomena*, 98:189–207, 1999.

[22] Blandine Jerome. Surface effects and anchoring in liquid crystals. *Reports on Progress in Physics*, 54(3):391, 1991.

[23] H Yokoyama and HA Van Sprang. A novel method for determining the anchoring energy function at a nematic liquid crystal-wall interface from director distortions at high fields. *Journal of applied physics*, 57(10):4520–4526, 1985.

[24] Hill De Vries. Rotatory power and other optical properties of certain liquid crystals. *Acta Crystallographica*, 4(3):219–226, 1951.

[25] Hirohisa Kawamoto. The history of liquid-crystal displays. *Proceedings of the IEEE*, 90(4):460–500, 2002.

[26] Stephen Palmer. Liquid-crystal cell with a wide viewing angle and a high cell contrast. *Applied optics*, 36(10):2094–2100, 1997.

[27] Ernst Lueder. *Liquid crystal displays: addressing schemes and electro-optical effects*. John Wiley & Sons, 2010.

[28] Nigel J Mottram and Christopher JP Newton. Introduction to q-tensor theory. *arXiv preprint arXiv:1409.3542*, 2014.

[29] Min Su Kim, Philip J Bos, Dong-Woo Kim, Deng-Ke Yang, Joong Hee Lee, and Seung Hee Lee. Flexoelectric effect in an in-plane switching (ips) liquid crystal cell for low-power consumption display devices. *Scientific reports*, 6:35254, 2016.

[30] Wang-Yang Li, Shu-Hsia Chen, et al. Simulation of normal anchoring nematic droplets under electrical fields. *Japanese Journal of Applied Physics*, 38(3A):1482–1487, 1999.

[31] James H Adler, Timothy J Atherton, DB Emerson, and Scott P MacLachlan. An energy-minimization finite-element approach for the frank–oseen model of nematic liquid crystals. *SIAM Journal on Numerical Analysis*, 53(5):2226–2254, 2015.

[32] JF Algorri, V Urruchi, PJ Pinzón, and JM Sánchez-Pena. Modeling electro-optical response of nematic liquid crystals by numerical methods. *Opt. Pura Aplicada*, 46(4):327–336, 2013.

[33] Filip Sala, Maksymilian Bujok, and Mirosław Karpierz. Modeling of molecular reorientation in nematic liquid crystals. *Photonics Letters of Poland*, 8(1):8–10, 2016.

[34] RD Polak, GP Crawford, BC Kostival, JW Doane, and S Žumer. Optical determination of the saddle-splay elastic constant k 24 in nematic liquid crystals. *Physical Review E*, 49(2):R978, 1994.

[35] A Kilian and Siegfried Hess. Derivation and application of an algorithm for the numerical calculation of the local orientation of nematic liquid crystals. *Zeitschrift für Naturforschung A*, 44(8):693–703, 1989.

[36] G Barbero, Z Gabbasova, and MA Osipov. Surface order transition in nematic liquid crystals. *Journal de Physique II*, 1(6):691–705, 1991.

[37] Eero Willman, F Aníbal Fernández, Richard James, and Sally E Day. Switching dynamics of a post-aligned bistable nematic liquid crystal device. *Journal of Display Technology*, 4(3):276–281, 2008.

[38] A Rapini and M Papoular. Distorsion d'une lamelle nématique sous champ magnétique conditions d'ancrage aux parois. *Le Journal de Physique Colloques*, 30(C4):C4–54, 1969.

[39] Jerzy Kedzierski, Zbigniew Raszewski, Edward Nowinowski-Kruszelnicki, Marek Andrzej Kojdecki, Wiktor Piecek, Paweł Perkowski, and Emilia Miszczyk. Composite method for measurement of splay, twist and bend nematic elastic constants by use of single special in-plane-switched cell. *Molecular Crystals and Liquid Crystals*, 544(1):57–1045, 2011.

[40] Pierre C Hohenberg and Bertrand I Halperin. Theory of dynamic critical phenomena. *Reviews of Modern Physics*, 49(3):435, 1977.

[41] Onno Bokhove and Jaap JW van der Vegt. Introduction to (dis) continuous galerkin finite element methods. *Department of Applied Mathematics, University of Twente*, 2005.

[42] Jerald L Ericksen. Conservation laws for liquid crystals. *Transactions of the Society of Rheology*, 5(1):23–34, 1961.

[43] Frank M Leslie. Some constitutive equations for liquid crystals. *Archive for Rational Mechanics and Analysis*, 28(4):265–283, 1968.

[44] Dwight W Berreman. Liquid-crystal twist cell dynamics with backflow. *Journal of Applied Physics*, 46(9):3746–3751, 1975.

[45] A Kilian and S Hess. On the simulation of the director field of a nematic liquid crystal. *Liquid Crystals*, 8(4):465–472, 1990.

[46] Fabrizio Di Pasquale, Hui Fang Deng, F Anibal Fernandez, Sally E Day, J Brian Davies, MT Johnson, AA Van der Put, JMA Van de Eerenbeemd, JAMM Van Haaren, and Jeff A Chapman. Theoretical and experimental study of nematic liquid crystal display cells using the in-plane-switching mode. *IEEE Transactions on Electron Devices*, 46(4):661–668, 1999.

[47] Apala Majumdar and Arghir Zarnescu. Landau–de gennes theory of nematic liquid crystals: the oseen–frank limit and beyond. *Archive for rational mechanics and analysis*, 196(1):227–280, 2010.

[48] BF De Oliveira, PP Avelino, F Moraes, and JCRE Oliveira. Nematic liquid crystal dynamics under applied electric fields. *Physical Review E*, 82(4):041707, 2010.

[49] PG Cummins, DA Dunmur, and DA Laidler. The dielectric properties of nematic 44 n-pentylcyanobiphenyi. *Molecular Crystals and Liquid Crystals*, 30(1-2):109–123, 1975.

[50] BR Ratna and R Shashidhar. Dielectric studies on liquid crystals of strong positive dielectric anisotropy. *Molecular Crystals and Liquid Crystals*, 42(1):113–125, 1977.

[51] Craig Maze. Determination of nematic liquid crystal elastic and dielectric properties from the shape of a capacitance-voltage curve. *Molecular Crystals and Liquid Crystals*, 48(3-4):273–287, 1978.

[52] J Jadzyn and P Kedziora. Anisotropy of static electric permittivity and conductivity in some nematics and smectics a. *Molecular crystals and liquid crystals*, 145(1):17–23, 1987.

[53] D Bauman and W Haase. Dielectric measurements of guest-host systems. *Molecular Crystals and Liquid Crystals*, 168(1):155–168, 1989.

[54] KT Schell and RS Porter. Dielectric studies of highly polar nematic liquid crystals and their mixtures. *Molecular Crystals and Liquid Crystals*, 188(1):97–103, 1990.

[55] OD Lavrentovich and VM Pergamenshchik. Stripe domain phase of a thin nematic film and the k 13 divergence term. *Physical review letters*, 73(7):979, 1994.

[56] David W Allender, GP Crawford, and JW Doane. Determination of the liquid-crystal surface elastic constant k 24. *Physical review letters*, 67(11):1442, 1991.

[57] A Sparavigna, OD Lavrentovich, and A Strigazzi. Periodic stripe domains and hybrid-alignment regime in nematic liquid crystals: Threshold analysis. *Physical Review E*, 49(2):1344, 1994.

[58] E Miraldi, C Oldano, and A Strigazzi. Periodic fréedericksz transition for nematic-liquid-crystal cells with weak anchoring. *Physical Review A*, 34(5):4348, 1986.

[59] Paul S Drzaic. *Liquid crystal dispersions*, volume 1. World Scientific, 1995.

[60] Roland1952. Structure of 4-cyano-4'-pentylbiphenyl. commons.wikimedia.org/wiki/File:4-Cyano-4Accessed: 2019-06-11.

[61] Tomasz to podludz. Mbba molecule. commons.wikimedia.org/wiki/File:MBBAcleaner.svg. Accessed: 2019-06-11.

[62] Shoyrudude555. Paa molecule. commons.wikimedia.org/wiki/File:Para-Azoxyanisole.png. Accessed: 2019-06-11.